Inorganic Chemistry

ARTICLE

pubs.acs.org/IC

Peptide-Bound Dinitrosyliron Complexes (DNICs) and Neutral/Reduced-Form Roussin's Red Esters (RREs/rRREs): Understanding Nitrosylation of [Fe−S] Clusters Leading to the Formation of DNICs and RREs Using a De Novo Design Strategy

Zong-Sian Lin,[†] Feng-Chun Lo,[†] Chih-Hsiang Li,[†] Chih-Hao Chen,[†] Wei-Ning Huang,[‡] I-Jui Hsu,[§] Jyh-Fu Lee,[⊥] Jia-Cherng Horng,[†] and Wen-Feng Liaw*[,†]

[†]Department of Chemistry, National Tsing Hua University, Hsinchu 30013, Taiwan

[‡]Department of Biotechnology, Yuanpei University, Hsinchu 30015, Taiwan

[§]Department of Molecular Science and Engineering, National Taipei University of Technology, Taipei 10608, Taiwan

[⊥]National Synchrotron Radiation Research Center (NSRRC), Hsinchu 30076, Taiwan

Supporting Information

ABSTRACT: This manuscript describes the interaction of low-molecular-weight DNICs with short peptides designed to explore the stability and structure of DNIC−peptide/RRE−peptide constructs. Although characterization of protein-bound and low-molecular-weight DNICs is possible via EPR, XAS, and NRVS, this study demonstrates that the combination of aqueous IR ν_{NO} and UV−vis spectra can serve as an efficient tool to characterize and discriminate peptide-bound DNICs and RREs. The de novo chelate-cysteine-containing peptides $KC(A)_nCK$-bound (n = 1−4) dinitrosyliron complexes $KC(A)_nCK$-DNIC (**CnA-DNIC**) and monodentate-cysteine-containing peptides KCAAK-/KCAAHK-bound Roussin's red esters (RREs) **KCAAK-RRE**/**KCAAHK-RRE** were synthesized and characterized by aqueous IR, UV−vis, EPR, CD, XAS, and ESI-MS. In contrast to the inertness of chelate-cysteine-containing peptide-bound DNICs toward KCAAK/KCAAHK, transformation of **KCAAK-RRE**/**KCAAHK-RRE** into **CnA-DNIC** triggered by **CnA** and reversible transformation between **CnA-DNIC** and **CnA-RRE** via $\{Fe(NO)_2\}^9$-$\{Fe(NO)_2\}^{10}$ reduced-form peptide-bound RREs demonstrate that the $\{Fe(NO)_2\}^9$ motif displays a preference for chelate-cysteine-containing peptides over monodentate-cysteine-containing peptides. Also, this study may signify that nitrosylation of [Fe−S] proteins generating protein-bound RREs, reduced protein-bound RREs, or protein-bound DNICs are modulated by both the oxidation state of iron and the chelating effect of the bound proteins of [Fe−S] clusters.

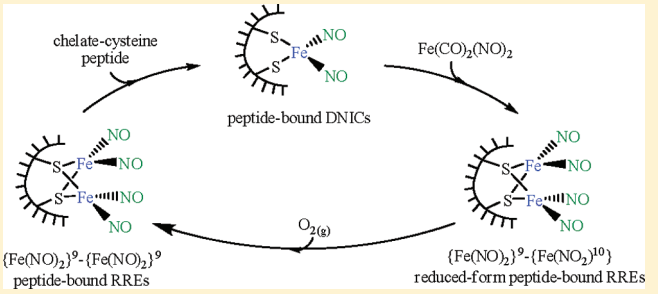

INTRODUCTION

Dinitrosyliron complexes (DNICs), the intrinsic NO-derived species existing in various NO-overproducing tissues,[1] and *S*-nitrosothiol are known as the two possible forms for storage and delivery of NO in a biological system.[2] Nitric oxide (NO) regulates multiple physiological reactions such as vasodilation, neuronal transmission, inflammation, immune system response, and cancer remedy.[3] NO in vivo can be stabilized and stored in the form of DNICs with proteins (protein-bound DNICs) and is probably released from cells in the form of low-molecular-weight DNICs (LMW-DNICs).[4] As has been known, characterization of both protein-bound DNICs and LMW-DNICs in vitro is possible via their distinctive electron paramagnetic resonance (EPR) signals at g = 2.03.[1−4]

A large number of metallopeptides, motivated by studies of electron transfer, the effect of metal-ion binding on protein folding/assembly and stability, catalytic function, electrochemistry, interactions with nucleic acid and the construction of structural analogues of the active sites of metalloproteins, have been designed and synthesized.[5] As has been known, de novo designed peptides can not only be considered as a bridge between metalloenzymes and organic model compounds but also may reveal both types of functions.[6] In particular, de novo designed peptides can regulate the metal−ligand-bonding interactions and tune the intrinsic properties of the metal centers.[7] For synthetic chemistry, one approach for mimicking the active site of reactive metalloenzymes to a thorough comprehension of their structural and functional roles in biology is to expand from traditional small-molecule biocoordination chemistry to the design and synthesis of peptide-based analogues, which were named "bridged biological assemblies".[8] The rational design of the stable de novo designed peptide-bound metal-ion active sites has shown remarkable success for the past decades.[8]

Received: July 19, 2011
Published: September 22, 2011

The peptide-based [4Fe−4S] synthetic analogue was synthesized to study the electron-transfer event and the midpoint reduction potentials of the [4Fe−4S] clusters regulated by proton-coupled cofactor.[9] In metallobiochemistry, the X-ray crystal structures of de novo apoprotein and metalated peptide, regarded as a basis to comprehend interaction between the metal ions and protein, were reported.[10] In addition, in the field of materials, de novo designed light-emissive peptide-bound porphyrin complexes have been synthesized based on the computational design.[11]

NO has been demonstrated to react with the [Fe−S] clusters of several proteins for regulating the physiological function of iron−sulfur protein.[112] The anaerobic reaction of high-potential iron protein (HiPIP) or NsrR, required for the upregulation of ResDE-dependent genes, with NO showed the generation of protein-bound DNICs.[4,13] Ding and co-workers showed that the ferredoxin [2Fe−2S] clusters were converted into protein-bound DNICs when *Escherichia coli* cells were treated with NO.[14] Lippard and co-workers demonstrated that the [2Fe−2S] clusters were nitrosylated to yield protein-bound Roussin's red esters (RREs) upon exposure of a Rieske-type ToMOC protein to NO.[15] Also, nitrosylation of WhiB-like protein containing a [4Fe−4S] cluster resulting in the formation of a protein-bound RRE was reported.[16]

S-Nitrosation, coupling of NO and a cysteine sulfur, has been identified as a post-translational modification of proteins to convey part of the ubiquitous influence of NO on thiol-dependent cellular-signaling transduction.[2] It is noticed that the NO motif of Cys-SNO in proteins may originate from GSNO (GS = glutathione), protein-bound SNO, NO-donor drugs, and HNO_2 derived from acidification of nitrite and DNICs.[2]

In chemistry, the $\{Fe(NO)_2\}$ motif coordinated by different ligands ($[SPh]^-$, $[-SC_4H_3S]^-$, $[C_3H_3N_2]^-$, $[OPh]^-$, and $[NO_2]^-$) displaying distinct electronic properties that are cooperatively regulated by the noninnocent NO ligands was concluded in the previous study.[17] The binding affinity of the coordinated ligands ($[SPh]^-$, $[-SC_4H_3S]^-$, $[C_3H_3N_2]^-$, $[OPh]^-$, and $[NO_2]^-$) toward the $\{Fe(NO)_2\}^9$ motif was also delineated. Of importance, the facile interconversion among $\{Fe(NO)_2\}^9$ DNICs, $[(NO)_2Fe(\mu\text{-SEt})_2Fe(NO)_2]$ RREs, and the $\{Fe(NO)_2\}^9$ $\{Fe(NO)_2\}^{10}$ reduced RREs (rRREs) $[(NO)_2Fe(\mu\text{-SEt})_2Fe(NO)_2]^-$ was demonstrated.[18] In addition, the redox shuttling between the $\{Fe(NO)_2\}^9$ and $\{Fe(NO)_2\}^{10}$ DNICs modulating the nitrite binding modes and then triggering nitrite activation to generate NO were identified.[19] Understanding the fundamental chemistry of biomimetic DNICs may provide new insights into the physiological process of NO storage and liberation. Efforts to look for an efficient tool to characterize and discriminate the existence of protein-bound DNICs/RREs/rRREs in a biological system led to the design and synthesis of peptide-bound DNICs/RREs. In this study, an anionic water-soluble DNIC, $[Fe(SPhNO_2COOH)_2(NO)_2]^-$ (**1**), and a series of short peptides containing cysteine(s) with the sequences KCACK (**C1A**), KCAACK (**C2A**), KCAAACK (**C3A**), KCAAAACK (**C4A**), KCAAK, and KCAAHK, respectively, were synthesized to study the binding affinity of chelate/monodenate-cysteine-containing peptides toward the $\{Fe(NO)_2\}^9$ motif. The UV−vis spectra and the aqueous IR ν_{NO} stretching frequencies/patterns of the peptide-bound DNICs/RREs/rRREs were demonstrated to be an efficient tool to characterize and discriminate the existence of peptide-bound DNICs/RREs/rRREs. In particular, a study of the transformation among peptide-bound DNICs, RREs, and rRREs may provide a way to understanding the nitrosylation products/pathways of [Fe−S] proteins, regulated by both the oxidation state of iron and the chelating effect of the bound proteins of [Fe−S] clusters in a biological system.

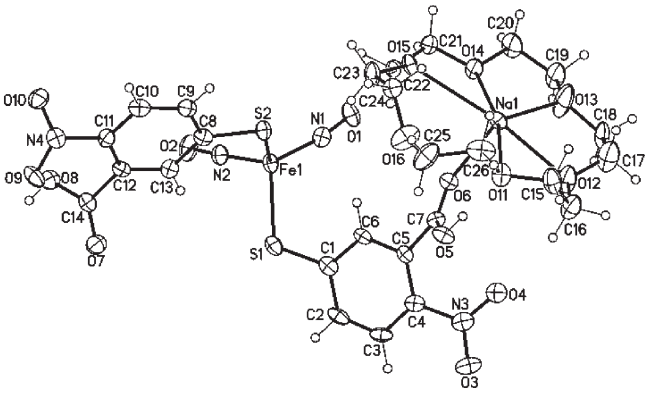

Figure 1. ORTEP drawing and labeling scheme of **1** in a [Na^+-18-crown-6-ether] salt with thermal ellipsoids drawn at 50% probability. Selected bond distances (Å) and angles (deg): Fe1−S1 2.2845(16), Fe1−S2 2.2879(16), Fe1−N1 1.688(5), Fe1−N2 1.681(5), N1−O1 1.173(6), N2−O2 1.176(6), Na1−O6 2.239(4); S1−Fe1−S2 112.33(6), N1−Fe1−N2 116.8(2).

RESULTS

Synthesis of [Na-18-Crown-6-ether][Fe(SPhNO$_2$COOH)$_2$(NO)$_2$] (1), a Water-Soluble DNIC. Upon the addition of 2 equiv of 5,5′-dithiobis(2-nitrobenzoic acid) into the CH_3CN solution of complex $[Fe_2(\mu\text{-S})_2(NO)_4]^{2-}$ at ambient temperature, a reaction ensued over the course of 30 min to yield the water-soluble $\{Fe(NO)_2\}^9$ DNIC **1**, characterized by IR, UV−vis, and single-crystal X-ray crystallography (Figure 1). The conversion of $[Fe_2(\mu\text{-S})_2(NO)_4]^{2-}$ to complex **1** was monitored by IR. The shift of IR ν_{NO} stretching frequencies from (1667 s, 1647 s cm^{-1}) to [1759 s, 1712 s cm^{-1} (ν_{NO}), 1732 s cm^{-1} (ν_{CO}, CH_3CN)] implicated the formation of complex **1**. The oxidative addition of 5,5′-dithiobis(2-nitrobenzoic acid) to $[Fe_2(\mu\text{-S})_2(NO)_4]^{2-}$ accompanied by reductive elimination of S_8 may rationalize the formation of complex **1**.

Syntheses of Peptides KCAAK, KCAAHK, KCACK (C1A), KCAACK (C2A), KCAAACK (C3A), and KCAAAACK (C4A). The differences of the binding affinity of ligands (thiolate, imidazolate, phenoxide, and nitrite) toward the $\{Fe(NO)_2\}^9$ motif, probed by ligand-substitution reactions, were demonstrated in the previous study.[17a] In order to understand the role(s) that the chelating effect of thiobiomolecules or proteins may play in creating/stabilizing the protein-bound DNICs/RREs and rationalizing the conversion of LMW-DNIC into protein-bound DNICs, the cysteinate-containing scaffold peptides (KCAAK, KCAAHK, **C1A**, **C2A**, **C3A**, and **C4A**) expected to bind to $\{Fe(NO)_2\}$ were synthesized. Alanine was selected as a spacer to separate two binding cysteinates, and the positively charged lysine was adopted to balance the negative charge of the DNIC core. The peptides containing 5−8 residues (KCAAK, **C1A**, **C2A**, **C3A**, and **C4A**) were synthesized by solid-phase methods using standard Fmoc protocols, purified by semipreparative high-performance liquid chromatography (HPLC) and identified by electrospray ionization mass spectrometry [ESI-MS; Figure S1 in the Supporting Information (SI)].[20]

Syntheses of De Novo Peptide-Bound DNICs C*n*A-DNIC (*n* = 1−4). Transformation of the water-soluble DNIC **1** into peptide-bound DNICs **C*n*A-DNIC** (n = 1−4) accompanied

Table 1. Aqueous IR ν_{NO} Stretching Frequencies, Electronic Absorption Bands, EPR Signals at 77 K, and Fe K-Edge XAS Preedge Energies for Peptide-Bound DNICs C*n*A-DNIC (n = 1−4) and RREs KCAAK-RRE/KCAAHK-RRE

	IR ν_{NO} (cm^{-1})	UV−vis (nm)	EPR (77 K)	preedge energy (eV)
C1A-DNIC	1722, 1767	309, 413	g_1 = 2.040, g_2 = 2.032, g_3 = 2.014	7113.4
C2A-DNIC	1722, 1768	313, 409	g_1 = 2.039, g_2 = 2.029, g_3 = 2.014	7113.7
C3A-DNIC	1720, 1767	315, 407	g_1 = 2.040, g_2 = 2.030, g_3 = 2.014	7113.7
C4A-DNIC	1721, 1766	313, 407	g_1 = 2.040, g_2 = 2.029, g_3 = 2.014	7113.7
KCAAK-RRE	1764, 1788, 1820	312, 366, 448		7113.7
KCAAHK-RRE	1764, 1788, 1820	310, 364, 448		
rC1A-RRE		310, 369, 464, 613, 952	$g_\perp$ = 2.006, $g_\parallel$ = 1.970	
rC2A-RRE		306, 368, 467, 646, 957	g_1 = 2.012, g_2 = 1.999, g_3 = 1.988	
rC3A-RRE		312, 367, 464, 639, 939	g_1 = 2.012, g_2 = 1.999, g_3 = 1.989	
rC4A-RRE		310, 370, 462, 637, 950	g_1 = 2.012, g_2 = 2.000, g_3 = 1.988	
C1A-RRE	1763, 1788, 1821	312, 366, 448		
C2A-RRE	1764, 1788, 1822	312, 364, 448		
C3A-RRE	1763, 1788, 1822	314, 366, 448		
C4A-RRE	1764, 1788, 1822	312, 364, 448		
complex **1**		400	g_1 = 2.036, g_2 = 2.029, g_3 = 2.022	
$[Fe(Cys)_2(NO)_2]^-$	1727, 1772	310, 405		

by the release of 3-carboxy-4-nitrobenzenethiolate ($[SPhNO_2$-$COOH]^-$ (a strong absorption band at 410 nm)) was observed when a phosphate buffer solution (pH 8.5) of complex **1** was treated with de novo peptides (**C1A**, **C2A**, **C3A**, and **C4A**, respectively) in a 1:1 molar ratio for 1 h at ambient temperature. All **C*n*A-DNIC** were purified by the gel-filtration chromatography (Bio-Gel P-2 Gel, Bio Rad). The **C*n*A-DNIC** were characterized by IR, UV−vis, EPR, and ESI-MS (Figure S2 in the SI and Table 1). The Fourier transform infrared (FTIR) spectra of peptide-bound DNICs **C*n*A-DNIC** in aqueous solution are depicted in Figures 2a and S3 in the SI. Compared to the thiolate-containing DNICs $[Fe(SEt)_2(NO)_2]^-$ displaying IR ν_{NO} (1674, 1715 cm^{-1}) in THF,[21] the aqueous IR ν_{NO} spectra of peptide-bound DNICs **C*n*A-DNIC** exhibit the diagnostic stretching frequencies 1722, 1767 cm^{-1} (**C1A-DNIC**), 1722, 1768 cm^{-1} (**C2A-DNIC**), 1720, 1767 cm^{-1} (**C3A-DNIC**), and 1721, 1766 cm^{-1} (**C4A-DNIC**), respectively (Table 1). In contrast to complex $[Fe(SPh)_2(NO)_2]^-$ dominated by intense absorption bands 479 and 798 nm in THF,[17c] the electronic spectra of peptide-bound DNICs **C*n*A-DNIC** display different patterns and absorptions in aqueous solution: 309 sh, 413 nm (**C1A-DNIC**), 313 sh, 409 nm (**C2A-DNIC**), 315 sh, 407 nm (**C3A-DNIC**), and 313 sh, 407 nm (**C4A-DNIC**) (Figures 3b and S4a,b in the SI). The UV−vis spectra of **C*n*A-DNIC** observed in this work are in very good accord with those published by Fontecave and co-workers using cysteamine as the thiol ligand.[17e]

EPR spectra of the peptide-bound DNICs **C*n*A-DNIC** are depicted in Figures 4a,b and S5b−d and S6b−d in the SI. At 77 K, **C1A-DNIC** displays a rhombic EPR signal at g_1 = 2.040, g_2 = 2.032, and g_3 = 2.014 (g_1 = 2.039, g_2 = 2.029, and g_3 = 2.014 for **C2A-DNIC**, g_1 = 2.040, g_2 = 2.030, and g_3= 2.014 for **C3A-DNIC**, and g_1 = 2.040, g_2 = 2.029, and g_3 = 2.014 for **C4A-DNIC**; Table 1). Intriguingly, the EPR spectrum of **C2A-DNIC** exhibits a well-resolved seven-line pattern with a g value of 2.029 (coupling constants $A_{N(NO)}$ = 2.45 G and $A_{H(Cys)}$ = 1.90 G) at 298 K. Compared to those of **C1A-DNIC**, **C3A-DNIC**, and **C4A-DNIC**, **C2A-DNIC** displays a seven-line EPR signal ascribed to the higher contribution of cysteine-containing peptide to the singly occupied molecular orbital of **C2A-DNIC**.[22] This could be further supported by the intense circular dichroism (CD) signals in the near-UV and visible regions (from 260 to 600 nm; Figure 5). In addition, the far-UV (from 200 to 260 nm) CD spectra indicate that these peptide-bound DNICs **C*n*A-DNIC** do not have significant secondary structures (Figure S7 in the SI).

Syntheses of De Novo Peptide-Bound RREs KCAAK-RRE and C*n*A-RRE (n = 1−4). Upon the addition of 1 equiv of $Fe(CO)_2(NO)_2$ to the aqueous solution of de novo monodentate-cysteine-containing peptide KCAAK at ambient temperature, the electronic absorption bands [312, 366, 448 sh nm (H_2O); Figure S4c in the SI] and IR ν_{NO} stretching frequencies [1764 s, 1788 s, 1820 w cm^{-1} (H_2O); Figure 2b] suggested formation of the peptide-bound RRE **KCAAK-RRE** containing two monodentate-cysteine-containing KCAAK peptides as bridging ligands (Figure S8a in the SI). Of importance, attempts to synthesize the de novo monodentate-cysteine-containing peptide-bound DNIC **$(KCAAK)_2$-DNIC** were unsuccessful by adding 2 equiv of KCAAK into a phosphate buffer (20 mM, pH = 8.5) of **KCAAK-RRE** at ambient temperature.[17e] In a similar fashion, the monodentate-cysteine-containing peptide-bound RRE **KCAAHK-RRE**, characterized by aqueous solution IR, UV−vis, and ESI-MS (Figure S8b in the SI and Table 1), was synthesized by the reaction of peptide KCAAHK and $Fe(CO)_2$-$(NO)_2$ at ambient temperature. The electronic absorption bands [310, 364, 448 sh nm (H_2O); Figure S4c in the SI] and IR ν_{NO} stretching frequencies [1764 s, 1788 s, 1820 w cm^{-1} (H_2O); Figure 2b] demonstrated the formation of monodentate-cysteine-containing peptide-bound RRE **KCAAHK-RRE**. The absence of formation of **KCAAHK-DNIC** with the cysteine-histidine-chelating mode is consistent with the binding affinity of coordinated ligands toward the $\{Fe(NO)_2\}^9$ motif observed in the biomimetic model study ($[SPh]^- > [-SC_4H_3S]^- > [C_3H_3$-$N_2]^- > [OPh]^- > [NO_2]^-$).[17a] The unique ability of the $[Fe(NO)_2]$ motif to bind chelate-cysteine-containing peptides **C*n*A** and monodentate-cysteine-containing peptide KCAAK provides the opportunity to probe the binding preference of the $[Fe(NO)_2]$ motif to **C*n*A** and KCAAK peptides. As shown in Scheme 1, upon the addition of 2 equiv of **C1A** to the aqueous

dx.doi.org/10.1021/ic201529e |*Inorg. Chem.* 2011, 50, 10417–10431

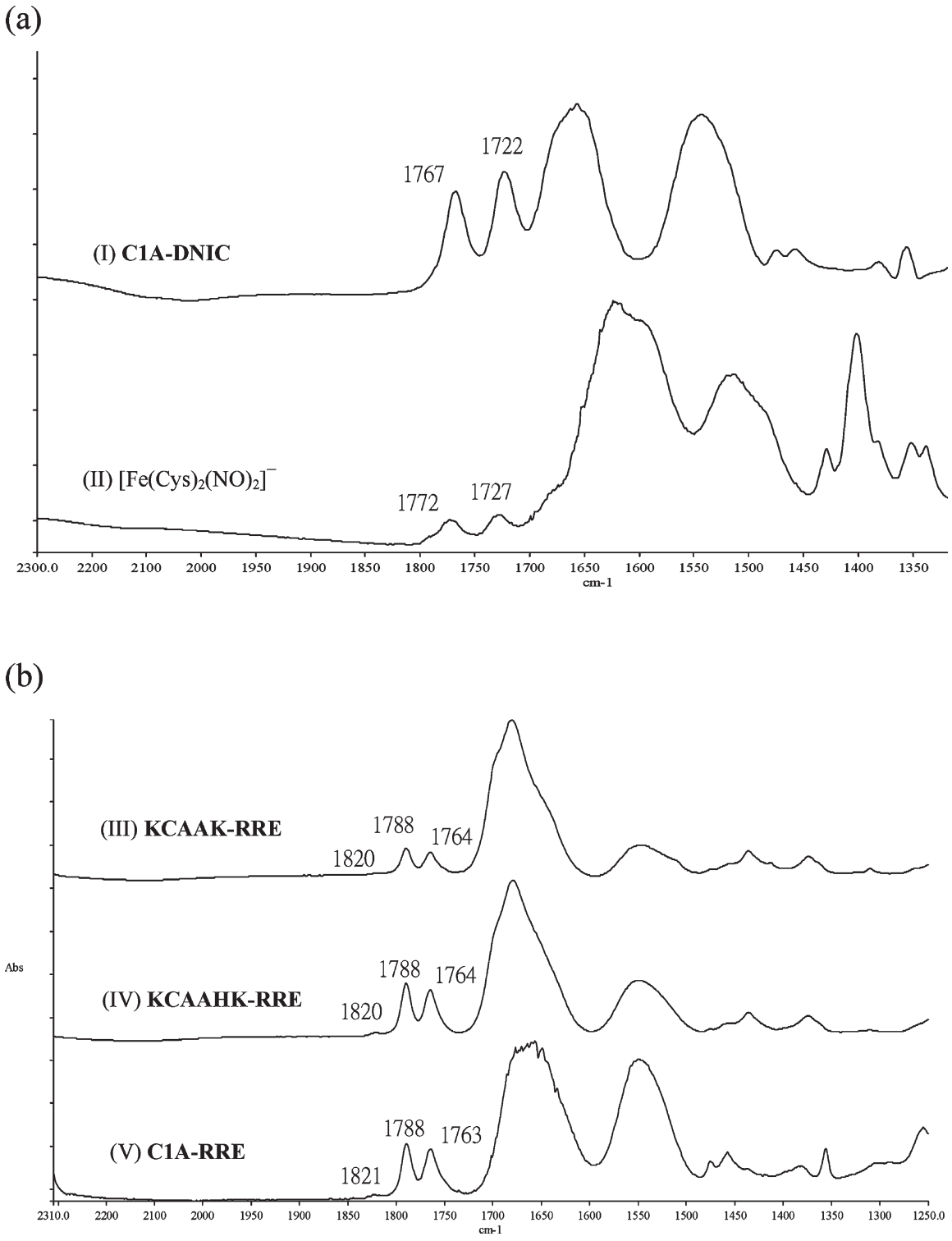

Figure 2. Aqueous IR ν_{NO} spectra (H_2O) of (a) (I) **C1A-DNIC** and (II) $[Fe(Cys)_2(NO)_2]^-$ and (b) (III) **KCAAK-RRE**, (IV) **KCAAHK-RRE**, and (V) **C1A-RRE**.

solution of **KCAAK-RRE** and stirring at ambient temperature for $^1/_2$ h, the IR ν_{NO} shift from [1764, 1788, 1820 cm^{-1} (H_2O)] to [1722, 1767 cm^{-1} (H_2O)] suggested formation of the chelate-cysteine-containing peptide-bound DNIC **C1A-DNIC**. However, the addition of 2 equiv of KCAAK to **C*n*A-DNIC** in aqueous solution reveals no detectable changes in IR ν_{NO} (Scheme 1).

In contrast to the inertness of **C*n*A-DNIC** toward KCAAK, the chelating peptides **C*n*A** triggering the transformation of **KCAAK-RRE** into peptide-bound DNICs **C*n*A-DNIC** implicates that the $[Fe(NO)_2]$ motif displays a preference for **C*n*A** over KCAAK (Scheme 1). The differences in the $[Fe(NO)_2]$ affinities for chelate-cysteine-containing peptide **C*n*A** and monodentate-cysteine-containing peptide KCAAK explain that

dx.doi.org/10.1021/ic201529e |*Inorg. Chem.* 2011, 50, 10417–10431

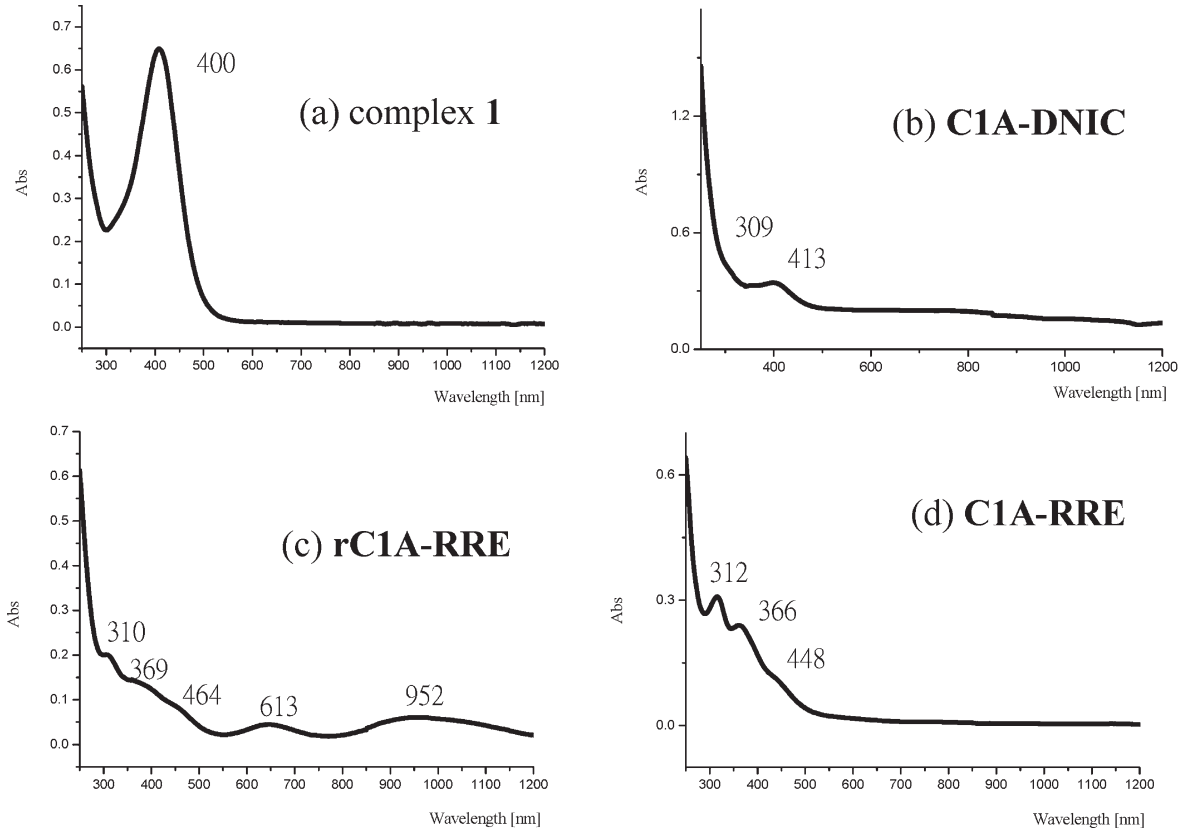

Figure 3. UV−vis spectra of (a) complex **1**, (b) **C1A-DNIC**, (c) **rC1A-RRE**, and (d) **C1A-RRE** in H_2O.

inclusion of the chelate-cysteine-containing peptide **C*n*A** may produce the more thermally stable $\{Fe(NO)_2\}^9$ DNICs (Scheme 1). This result rationalizes the failure of isolation of the monodentate-cysteine-containing peptide-bound DNIC and opens an avenue for the synthesis of chelate-cysteine-containing peptide-bound RREs.

As shown in Scheme 2a,b, chelate-cysteine-containing peptide-bound RREs **C*n*A-RRE** (n = 1−4) were synthesized by reacting peptide-bound DNICs **C*n*A-DNIC** with $Fe(CO)_2(NO)_2$ in aqueous solution at ambient temperature followed by contact with O_2. The transformation of peptide-bound DNICs **C*n*A-DNIC** into peptide-bound RREs **C*n*A-RRE** via the $\{Fe(NO)_2\}^9\{Fe(NO)_2\}^{10}$ reduced peptide-bound RRE **rC*n*A-RRE** was monitored by UV−vis spectra in aqueous solution; the shift of the electronic bands from 309 sh, 413 nm [**C1A-DNIC** (H_2O); Figure 3b] to 310, 369, 464, 613, 952 nm (**rC1A-RRE**; Figures 3c and S4d in the SI) and then a further shift to [312, 366, 448 sh nm (H_2O); **C1A-RRE**; Figures 3d and S4b in the SI] confirmed the conversion of **C1A-DNIC** to **C1A-RRE** via the reduced-form **rC1A-RRE** (Table 1). In EPR spectra, the disappearance of a rhombic EPR signal at g_1 = 2.040, g_2 = 2.032, and g_3 = 2.014 [**C1A-DNIC** (H_2O); Figures 4b and S6 in the SI] accompanied by the simultaneous formation of the signal at $g_\perp$ = 2.006 and $g_\parallel$ = 1.970 [**rC1A-DNIC** (H_2O); Figures 4c and S9 in the SI] also confirmed formation of the $\{Fe(NO)_2\}^9\{Fe(NO)_2\}^{10}$ reduced peptide-bound RRE **rC1A-RRE** when **C1A-DNIC** was reacted with $Fe(CO)_2(NO)_2$ in aqueous solution at ambient temperature. All peptide-bound RREs **KCAAK-RRE** and **C*n*A-RRE** were purified by gel-filtration chromatography (Bio-Gel P-2 Gel, Bio Rad) and identified by ESI-MS (Figure S10 in the SI). In comparison with RRE $[Fe(SEt)(NO)_2]_2$ showing IR ν_{NO} 1749 s, 1774 s, 1809 w cm^{-1} in THF,[23] aqueous IR ν_{NO} spectra of peptide-bound RREs **C*n*A-RRE** exhibit the diagnostic stretching frequencies 1763 s, 1788 s, 1821 w cm^{-1} (**C1A-RRE**), 1764 s, 1788 s, 1822 w cm^{-1} (**C2A-RRE**), 1763 s, 1788 s, 1822 w cm^{-1} (**C3A- RRE**), and 1764 s, 1788 s, 1822 w cm^{-1} (**C4A-RRE**) in H_2O, respectively (Figures 2b and S11 in the SI). It is noticed that the separation ($\Delta\nu_{NO}$ = ∼45 cm^{-1}) of ν_{NO} stretching frequencies of the peptide-bound DNICs **C*n*A-DNIC** is different from that ($\Delta\nu_{NO}$ = ∼25 cm^{-1}) of peptide-bound RREs **C*n*A-RRE** (Table 1).

In particular, conversion of chelate-cysteine-containing peptide-bound RREs **C*n*A-RRE** to chelate-cysteine-containing peptide-bound DNICs **C*n*A-DNIC** was displayed when 1 equiv of peptide **C*n*A** was added to the phosphate buffer (20 mM, pH 8.5) solution of **C*n*A-RRE** at ambient temperature (Scheme 2c). These results illustrate that the transformation pathway of **C*n*A-DNIC** into **C*n*A-RRE** exclusively occurs via the intermediate **rC*n*A-RRE**. In contrast, **C*n*A** peptides trigger the direct conversion of **C*n*A-RRE** to **C*n*A-DNIC** in aqueous solution at ambient temperature, as shown in Scheme 2. This study demonstrates that the $\{Fe(NO)_2\}^9$ motif shows a strong preference for the formation of chelate-cysteine-containing peptide-bound DNICs over the formation of chelate-cysteine-containing peptide-bound RREs.

Of importance, we noticed that the combination of UV−vis spectra of the peptide-bound RRE **C*n*A-RRE** (or **KCAAK-RRE**) and peptide-bound DNIC **C*n*A-DNIC** is almost the same as the UV−vis spectrum [absorption bands 310, 360, 410 nm (H_2O)] derived from nitrosylation of *Fur. E. coli* (containing four cysteines),[24]

dx.doi.org/10.1021/ic201529e |*Inorg. Chem.* 2011, 50, 10417–10431

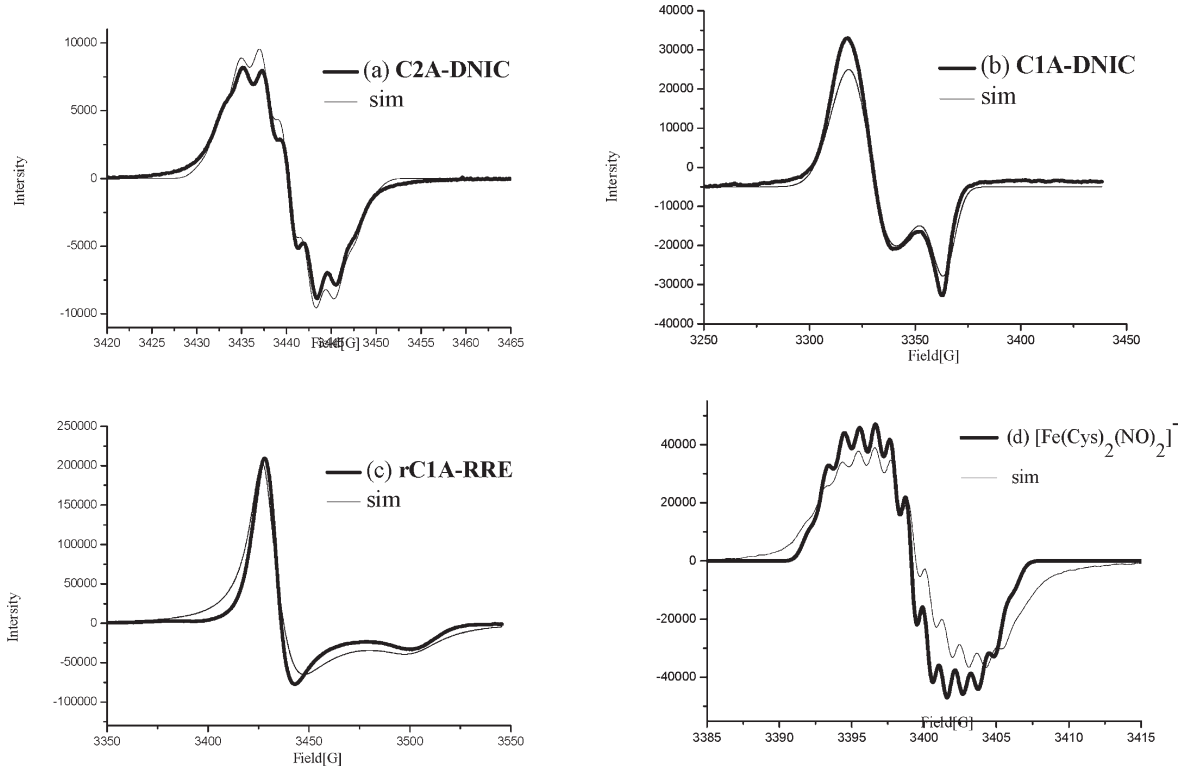

Figure 4. EPR spectra (H_2O) of (a) **C2A-DNIC** with $g = 2.029$ ($A_{(N)} = 2.45$ G; $A_{(H)} = 1.90$ G) at 298 K, (b) **C1A-DNIC** with $g_1 = 2.040$, $g_2 = 2.032$, and $g_3 = 2.014$ at 77 K, (c) **rC1A-RRE** with $g_\perp = 2.006$ and $g_\parallel = 1.970$ at 77 K, and (d) $[Fe(Cys)_2(NO)_2]^-$ with $g = 2.031$ ($A_{(N)} = 2.2$ G; $A_{(H)} = 1.18$ G) at 298 K.

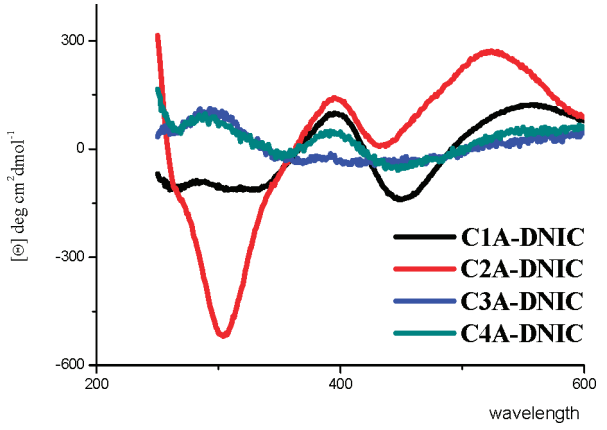

Figure 5. CD spectra for **C*n*A-DNIC** (n = 1−4) at 298 K. All measurements were conducted in the aqueous solution.

assigned to the combination of protein-bound $\{Fe(NO)_2\}^9$ ($S = {}^1/_2$) and $\{Fe(NO)_2\}^8$ ($S = 0$) DNICs.[24] Also, the combination of IR ν_{NO} spectra of the peptide-bound RRE **C*n*A-RRE** (or **KCAAK-RRE**) and peptide-bound DNIC **C*n*A-DNIC**, identical with the IR ν_{NO} spectra of nitrosylation of *Fur. E. coli* (IR ν_{NO} stretching frequencies 1718, 1765, 1787, and 1815 cm^{-1}),[24] suggests that nitrosylation of *Fur. E. coli* may produce a mixture of protein-bound DNICs and RREs. Therefore, in addition to EPR, X-ray absorption spectroscopy (XAS), and nuclear resonance vibrational spectroscopy (NRVS) reported to be adopted to characterize DNICs and RREs,[22,25] it is presumed that aqueous solution FTIR ν_{NO} spectra in combination with UV−vis spectra may serve as an efficient tool for characterization and discrimination of the $\{Fe(NO)_2\}^9$ DNICs,

Scheme 1

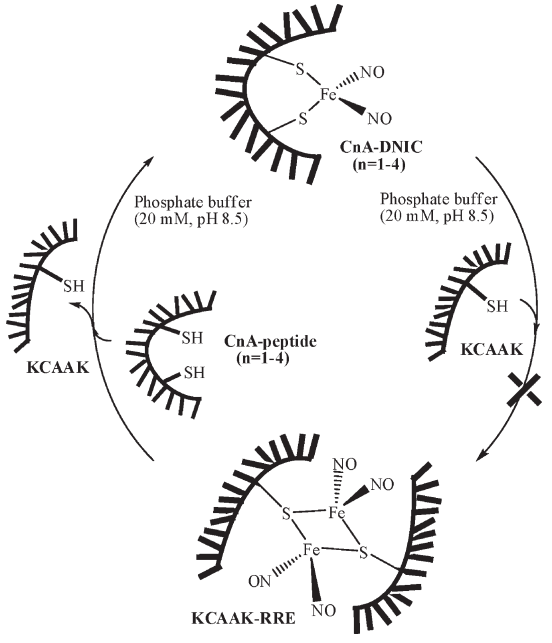

$\{Fe(NO)_2\}^9$-$\{Fe(NO)_2\}^{10}$ rRREs, and $\{Fe(NO)_2\}^9\{Fe(NO)_2\}^9$ RREs in biology.

Transfer of the $\{Fe(NO)_2\}$ Core of Cysteine-Containing Peptide-Bound DNICs and RREs. Transfer of the $\{Fe(NO)_2\}^9$ core of peptide-bound DNICs was also investigated by the

dx.doi.org/10.1021/ic201529e |*Inorg. Chem.* 2011, 50, 10417–10431

Scheme 2

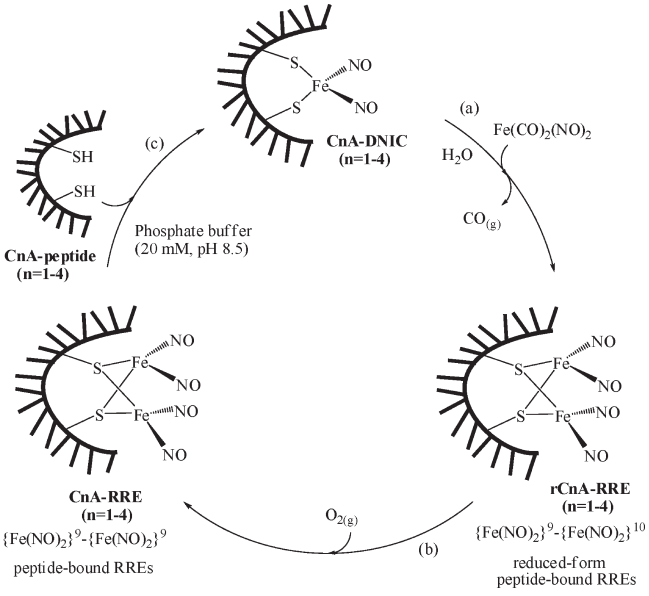

reaction of peptide-bound DNICs **C1A-DNIC** and peptide **C*n*A** (n = 2−4; or LMW cysteine) under N_2 in aqueous solution at ambient temperature (Scheme 3). In contrast to the inertness of peptide-bound DNICs **C*n*A-DNIC** toward free cysteine (Scheme 4a), the coexistence of **C1A-DNIC** and **C2A-DNIC** was observed when **C1A-DNIC** was reacted with 1 equiv of **C2A** in aqueous solution at ambient temperature (Figure S12 in the SI and Scheme 3). As shown in Scheme 4, the relative stability of **C*n*A-DNIC** (n = 1−4), **KCAAK-RRE**, and **C*n*A-RRE** (n = 1−4) toward free cysteine was determined through the addition of free cysteine to an aqueous solution of **C*n*A-DNIC**, **KCAAK-RRE**, and **CnA-RRE**, respectively, at ambient temperature. The addition of 4 equiv of cysteine into an aqueous solution of monodentate-cysteine-containing peptide-bound RREs **KCAAK-RRE** resulted in the formation of DNIC $[Fe(Cys)_2(NO)_2]^-$ characterized by the aqueous solution IR ν_{NO} (stretching frequencies at 1727 and 1772 cm^{-1}; Figure 1a), UV−vis (electronic absorption bands at 308 and 408 nm; Figure S2e in the SI), and EPR (a well-resolved 13-line hyperfine-splitting EPR g value of 2.031 with coupling constants $A_{N(NO)}$= 2.2 G and $A_{H(Cys)}$= 1.18 G) spectra at 298 K (Figure 4d and Table 1).[26] In contrast, the reaction of **C*n*A-RRE** (n = 1−4) and cysteine in a 1:2 stoichiometry yielded **C*n*A-DNIC** and $[Fe(Cys)_2(NO)_2]^-$, identified by aqueous solution IR, UV−vis, EPR, and ESI-MS (Scheme 4c). These results illustrate one aspect of how the peptide-bound DNICs/RREs function as an $[Fe(NO)_2]$-donor species in the presence of chelate-cysteine-containing peptides and free cysteine. Also, it is concluded that the relative stability of **C*n*A-DNIC**, **KCAAK-RRE**, and **C*n*A-RRE** toward free cysteine follows the order of **C*n*A-DNIC** > **C*n*A-RRE** > **KCAAK-RRE**. That is, the binding affinity of chelate-cysteine-containing peptide **C*n*A**, free cysteine, and monodentate-cysteine-containing peptide **KCAAK** toward the $\{Fe(NO)_2\}^9$ motif leading to the formation of DNICs is in the order of chelate-cysteine-containing peptide > free cysteine ≫ monodentate-cysteine-containing peptide. This order, presumably, is related to the chelating effect of the bound peptides.

Scheme 3

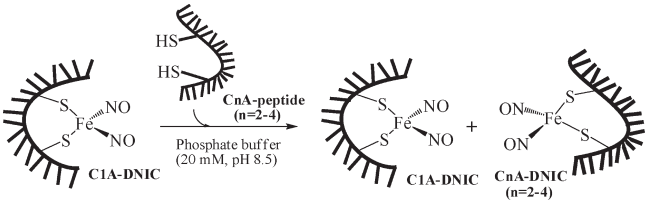

Scheme 4

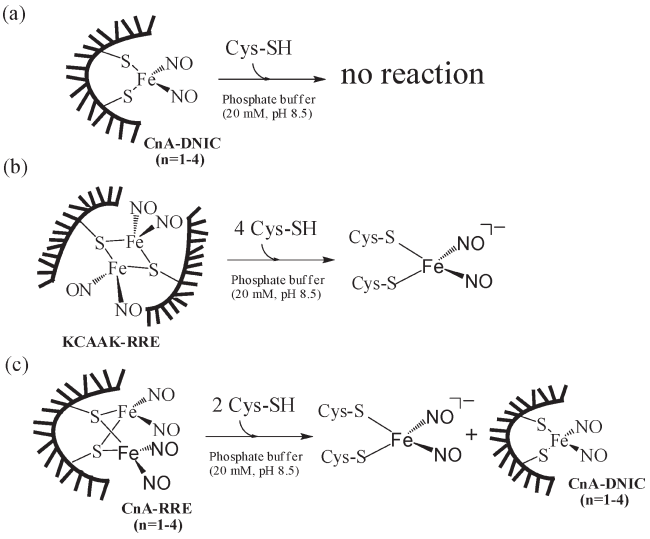

Fe K-Edge XAS Studies of Peptide-Bound DNICs C*n*A-DNIC (n = 1−4) and RRE KCAAK-RRE. To clarify the local structures of a series of chelate-cysteine-containing peptide-bound DNICs **C*n*A-DNIC** and monodentate-cysteine-containing peptide-bound RRE **KCAAK-RRE**, we conducted XAS measurements. The experimental Fe K-edge spectra of peptide-bound DNIC **C4A-DNIC**, RRE **KCAAK-RRE**, and model complexes ($[Fe(SEt)_2(NO)_2]^-$ and $[Fe(SEt)(NO)_2]_2$) were depicted in Figure 6. All peptide-bound DNICs **C*n*A-DNIC** display the obvious peak within the range of 7113.4−7113.8 eV (Table 1),[17a] which is generally assigned as a 1s → 3d transition. On the basis of the Laporte selection rule,[27] transitions are forbidden if two states have the same parity. The relatively strong preedge intensities indicate that the local geometry of the Fe center is in a noncentrosymmetric environment (such as tetrahedral symmetry, T_d). In T_d symmetry, σ bonding between a transition metal and a ligand can be described as the mixing of metal orbitals of sp^3 with sd^3 hybridization. The mixing of a p orbital (u parity) with a d orbial to relax the Laporte selection rule rationalizes that the strong preedge peak within the range of 7113.4−7113.8 eV was observed. This implies that the local environment of the Fe site is bound by four-coordinated atoms.

Extended X-ray absorption fine structure (EXAFS) data analysis was performed to obtain the local structure of the Fe site of peptide-bound DNICs **C*n*A-DNIC** and RRE **KCAAK-RRE**, respectively (Figures 7 and S13 in the SI). The k^3-weighted EXAFS raw data ($k^3\chi$) used in the data analysis are displayed in the inset. The fitting results are listed in Table S2 in the SI.

dx.doi.org/10.1021/ic201529e |*Inorg. Chem.* 2011, 50, 10417–10431

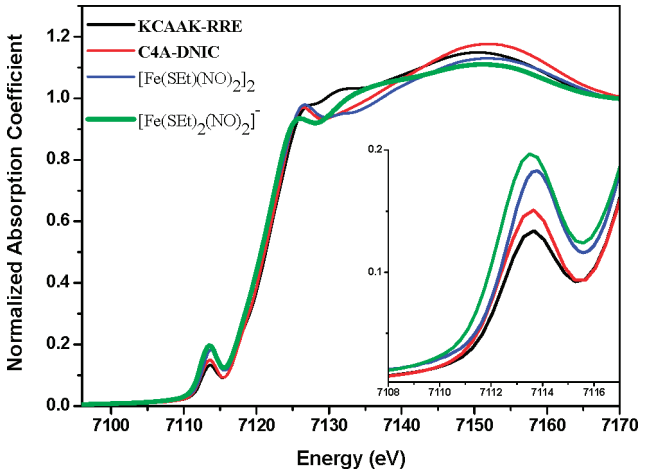

Figure 6. Normalized XANES at the Fe K-edge of **C4A-DNIC**, **KCAAK-RRE**, and model compounds ($[Fe(SEt)_2(NO)_2]^-$ and $[Fe(SEt)_2(NO)_2]_2$). The enlarged preedge region is depicted in the inset.

The EXAFS fitting results of peptide-bound DNICs **C*n*A-DNIC** indicate that the Fe is bound with two N and two S atoms at average distances of 1.68−1.70 and 2.26−2.30 Å, respectively. The third peak in the radial distribution function, including the multiple scattering contribution of Fe−N−O, is assigned as the distance between Fe and O (2.80−2.82 Å). The EXAFS data and fitting results are consistent with our previous single-crystal structures of DNIC models.[17a,28] In the peptide-bound RRE **KCAAK-RRE**, the first and second peaks in the radial distribution function arise mainly from backscattering from two ligated N atoms and two ligated S atoms, respectively. The third peak in the radial distribution function is dominated by the single scattering path between Fe and Fe as well as multiple scattering contributions from the Fe−N−O path. The EXASF result of peptide-bound RRE **KCAAK-RRE** is best described as a $[Fe(\mu\text{-}S_{Cys})_2Fe]$ core with NO molecules coordinated to two Fe sites. The average Fe−N, Fe−S, Fe---Fe, and Fe---O distances are calculated as 1.70(2), 2.27(1), 2.70(1), and 2.76(3) Å, respectively, consistent with those of $[Fe(SEt)(NO)_2]_2$ obtained from the single-crystal X-ray structure.[29]

DISCUSSION

Characterization of the nitrosylation products of [Fe−S] proteins in biological systems has been intensively studied.[12−16] As shown in Schemes 1−4, the study on the binding affinity of chelate/monodentate-cysteine-containing peptides toward the $[Fe(NO)_2]$ motif and the transformation among chelate/monodentate-cysteine-containing peptide-bound RREs, chelate-cysteine-containing peptide-bound DNICs, and free-cysteine-containing DNIC may lend credence to the proposal that nitrosylation of [Fe−S] proteins generates protein-bound RREs, reduced protein-bound RREs, or protein-bound DNICs, modulated by both the oxidation state of iron and the chelating effect of the bound proteins of [Fe−S] clusters, although in most cases proteins are not structurally altered to a great extent upon interaction with NO in vivo. Also, the local sequence of the proteins are hardly similar to the peptide sequences used in this study. This biomimetic study leading to initial insights concerning the degradation pathways and products of nitrosylating [Fe−S] proteins may be further classified as follows:

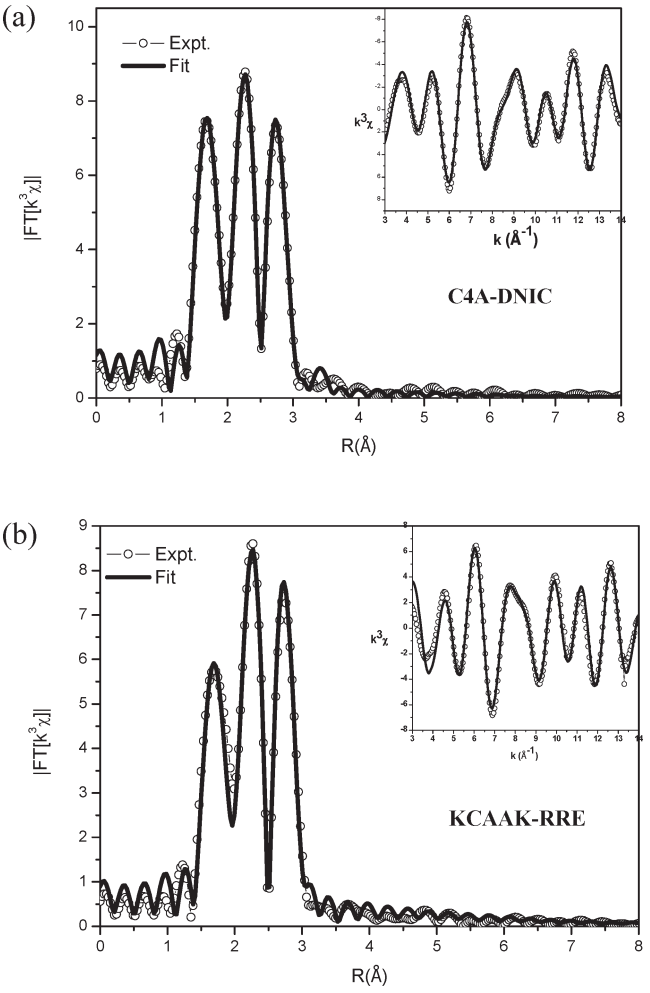

Figure 7. EXAFS data ($k^3\chi$ shown in the inset) and the Fourier transforms for (a) **C4A-DNIC** and (b) **KCAAK-RRE**. Open circles and solid lines denote the experimental data and fitting results, respectively.

a. Nitrosylation of the Oxidized/Reduced-Form [1Fe−0S] Rubredoxin Bound by Monodentate-Cysteine-Containing Proteins. As observed in the previous biomimetic study,[21] nitrosylation of the oxidized/reduced-form [1Fe−0S] rubredoxin bound by monodentate-cysteine-containing proteins may lead to the proposed thermally unstable $\{Fe(NO)_2\}^9$ monodentate-cysteine-containing protein-bound DNIC **A** intermediate via the reductive elimination of disulfide and cysteine-containing protein (Scheme 5).[18a] This highly unstable $\{Fe(NO)_2\}^9$ DNIC **A** intermediate is then driven to yield the $\{Fe(NO)_2\}^9$-$\{Fe(NO)_2\}^9$ monodentate-cysteine-containing protein-bound RREs via the elimination of cysteine-containing protein (Scheme 5).

b. Nitrosylation of the Oxidized/Reduced-Form [1Fe−0S] Rubredoxin Bound by Chelate-Cysteine-Containing Proteins. Instead of formation of the protein-bound RREs derived from nitrosative degradation of the monodentate-cysteine-containing [1Fe−0S] rubredoxin, nitrosylation of the oxidized/reduced-form [1Fe−0S] rubredoxin bound by chelate-cysteine-containing proteins was presumed to lead to formation of the thermally stable $\{Fe(NO)_2\}^9$ chelate-cysteine-containing protein-bound DNICs along with the reductive elimination of disulfide and elimination of the proposed chelate-cysteine-containing protein,

Scheme 5

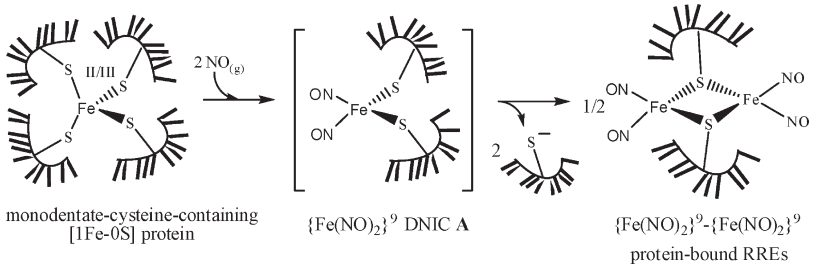

respectively (Scheme 6a,b). This study shows that the thermal stability of peptide-bound DNICs/RREs is on the order of bidentate-cysteine-containing peptide-bound DNICs > bidentate-cysteine-containing peptide-bound RREs. Conclusively, the formation of protein-bound RREs or protein-bound DNICs derived from nitrosylation of the oxidized/reduced-form [1Fe−0S] rubredoxin is, obviously, regulated by the chelating effect of the bound proteins of [Fe−S] clusters.

c. Nitrosylation of the Oxidized/Reduced-Form Monodentate-Cysteine-Containing [2Fe−2S] Ferredoxin. As shown in Scheme 7a,[28] nitrosylation of the monodentate-cysteine-containing oxidized-form [2Fe−2S] ferredoxin yielded $\{Fe(NO)_2\}^9$-$\{Fe(NO)_2\}^9$ protein-bound RREs accompanied by elimination of sulfide via the thermally unstable $\{Fe(NO)_2\}^9$ monodentate-cysteine-containing protein-bound DNICs. As observed in the biomimetic study,[21] NO radical binding to the electron-deficient Fe^{III}−Fe^{II} center of the reduced-form monodentate-cysteine-containing [2Fe−2S] ferredoxin may trigger reductive elimination of sulfide accompanied by formation of the thermally unstable $\{Fe(NO)_2\}^9$ and $\{Fe(NO)_2\}^{10}$ monodentate-cysteine-containing DNICs (Scheme 7b). The coordinative association of the $\{Fe(NO)_2\}^9$ and $\{Fe(NO)_2\}^{10}$ DNICs leading to the dinuclear $\{Fe(NO)_2\}^9$-$\{Fe(NO)_2\}^{10}$ reduced-form protein-bound RRE intermediate followed by subsequent oxidation of the assembled reduced-form protein-bound RRE intermediate rationalizes formation of the $\{Fe(NO)_2\}^9$-$\{Fe(NO)_2\}^9$ monodentate-cysteine-containing RREs (Scheme 7b), supported by nitrosylation of Rieske-type [2Fe−2S] ferredoxin ToMOC protein including two histidine (His 45 and His 67) and two cysteine (Cys 47 and Cys 64) ligands, yielding protein-bound RRE, reported by Lippard and co-workers.[15]

d. Nitrosylation of the Oxidized/Reduced-Form Chelate-Cysteine-Containing [2Fe−2S] Ferredoxin. In contrast to nitrosylation of the monodentate-cysteine-containing [2Fe−2S] ferredoxin producing the $\{Fe(NO)_2\}^9$-$\{Fe(NO)_2\}^9$ protein-bound RREs, nitrosylation of the oxidized-form chelate-cysteine-containing [2Fe−2S] ferredoxin was proposed to yield the thermally stable $\{Fe(NO)_2\}^9$ chelate-cysteine-containing protein-bound DNICs (Scheme 8a). In a similar fashion, nitrosylation of the reduced-form chelate-cysteine-containing [2Fe−2S] ferredoxin was presumed to generate the thermally stable $\{Fe(NO)_2\}^9$ chelate-cysteine-containing protein-bound DNICs via a consecutive process, oxidation of the reduced-form protein-bound RREs and the subsequent splitting of $\{Fe(NO)_2\}^9$-$\{Fe(NO)_2\}^9$ protein-bound RREs (Scheme 8b). In the biological study,[14] nitrosylation of a reduced-form SoxR protein-containing [2Fe−2S] cluster leads to the formation of protein-bound DNICs.

e. Nitrosylation of the Cysteine-Containing [4Fe−4S]$^{2+}$ Ferredoxin. In contrast to nitrosylation of the chelate-cysteine-containing [1Fe−0S]/[2Fe−2S] producing protein-bound

Scheme 6

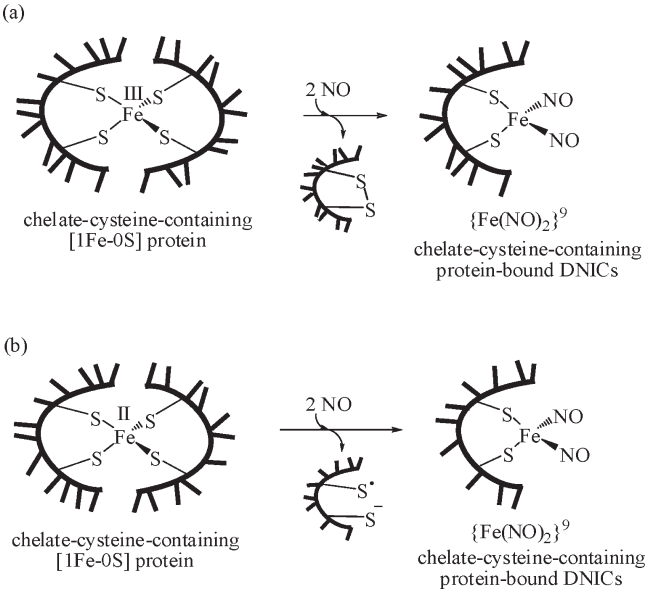

DNICs, nitrosylation of chelate-cysteine-containing $[4Fe−4S]^{2+}$ ferredoxin may exclusively yield protein-bound RREs via the $\{Fe(NO)_2\}^9$-$\{Fe(NO)_2\}^{10}$ reduced-form protein-bound RRE intermediate (Scheme 9a). Compared to nitrosylation of the monodentate-cysteine-containing [1Fe−0S]/[2Fe−2S] yielding protein-bound RREs, nitrosylation of monodentate-cysteine-containing $[4Fe−4S]^{2+}$ ferredoxin is presumed to result in the formation of protein-bound RREs via the $\{Fe(NO)_2\}^9$-$\{Fe(NO)_2\}^{10}$ reduced-form protein-bound RRE intermediate (Scheme 9b), supported by nitrosylation of the [4Fe−4S] protein (bound by four cysteines, Cys 23, Cys 53, Cys 56, and Cys 62) in a WhiB-like family (WhiD), yielding protein-bound RREs reported by Le Brun and co-workers.[16]

■ CONCLUSION AND COMMENTS

Syntheses of the cysteine-containing peptide-bound DNICs/RREs/rRRE and study on the peptide-substitution reactions among cysteine-containing peptide-bound DNICs, cysteine-containing peptide-bound RREs, and free-cysteine-bound DNICs have led to the following results.

1 The chelate-cysteine-containing peptide-bound DNICs, characterized by aqueous solution IR, UV−vis, ESI-MS, EPR, and CD spectra and XAS measurements, were

dx.doi.org/10.1021/ic201529e |Inorg. Chem. 2011, 50, 10417–10431

Scheme 7

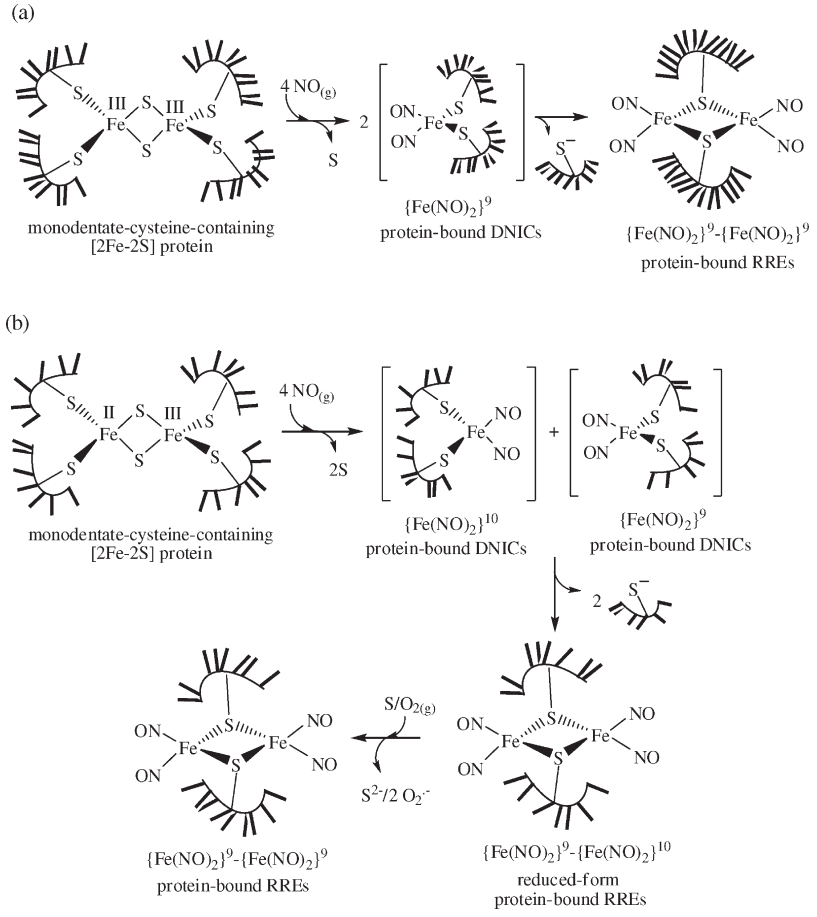

synthesized by the reaction of anionic water-soluble DNIC **1** and peptides **C*n*A**. In contrast, the chelate-cysteine-containing peptide-bound RREs were prepared by the reaction of $\{Fe(NO)_2\}^{10}$ $[Fe(CO)_2(NO)_2]$ and peptide-bound DNICs **C*n*A-DNIC** (n = 1−4) followed by O_2 oxidation. As shown in Schemes 1 and 2, chelate-cysteine-containing peptide-bound RREs and DNICs are chemically reversible, in contrast to the irreversibility between monodentate-cysteine-containing peptide-bound RREs and chelate-cysteine-containing peptide-bound DNICs.

2 It is noticed that the IR ν_{NO} spectra of monodentate-cysteine-containing peptide-bound RRE **KCAAK-RRE** and chelate-cysteine-containing peptide-bound RREs **C*n*A-RRE** had the same pattern/position and the similar separation of NO stretching frequencies ($\Delta\nu_{NO}$) (1764 s, 1788 s, 1820 w cm^{-1} with $\Delta\nu_{NO}$ = ∼24 cm^{-1} (H_2O) for **KCAAK-RRE** and 1763 s, 1788 s, 1821 w cm^{-1} with $\Delta\nu_{NO}$ = ∼25 cm^{-1} for **C1A-RRE** in aqueous solution). In contrast to separation ($\Delta\nu_{NO}$) of the NO stretching frequencies of ∼24 cm^{-1} (H_2O) for peptide-bound RREs containing chelate/monodentate cysteines, the chelate-cysteine-containing peptide-bound DNIC **C*n*A-DNIC** displays diagnostic ν_{NO} stretching frequencies [e.g., 1722 s, 1767 s cm^{-1} (H_2O) for **C1A-DNIC**] with a separation ($\Delta\nu_{NO}$) of the NO stretching frequencies of ∼45 cm^{-1}. In conclusion, the relative position of the ν_{NO} stretching frequencies of aqueous solution IR ν_{NO} spectra in combination with the pattern of aqueous IR ν_{NO} spectra may serve as an efficient tool to characterize and discriminate the existence of protein-bound DNICs and RREs in a biological system, in addition to EPR, XAS, and NRVS.[23,26]

3 The binding affinity of chelate-cysteine-containing peptides and monodentate-cysteine-containing peptide toward the $[Fe(NO)_2]$ motif may implicate that the stability of peptide-bound/cysteine-bound RREs/DNICs is on the order of bidentate-cysteine-containing peptide-bound DNICs > free-cysteine-bound DNIC ≫ monodentate-cysteine-containing peptide-bound DNICs. Transformation of **C*n*A-RRE** into **C*n*A-DNIC** under the presence of **C*n*A** explains to some extent the stability of bidentate-cysteine-containing peptide-bound DNICs over bidentate-cysteine-containing peptide-bound RREs (∼monodentate-cysteine-containing peptide-bound RREs). Namely, it is important not only that chelate-cysteine-containing peptides stabilize the DNIC form but also that chelate-cysteine-containing peptides destabilize the RRE form.

Our results bridging the peptide-substitution reaction study and investigation of the transformation between peptide-bound RREs and DNICs may point the way to understanding nature's choice of forming chelate-cysteine-containing protein-bound DNICs/RREs and monodentate-cysteine-containing protein-bound RREs. That is, the results described in this study speak

Scheme 8

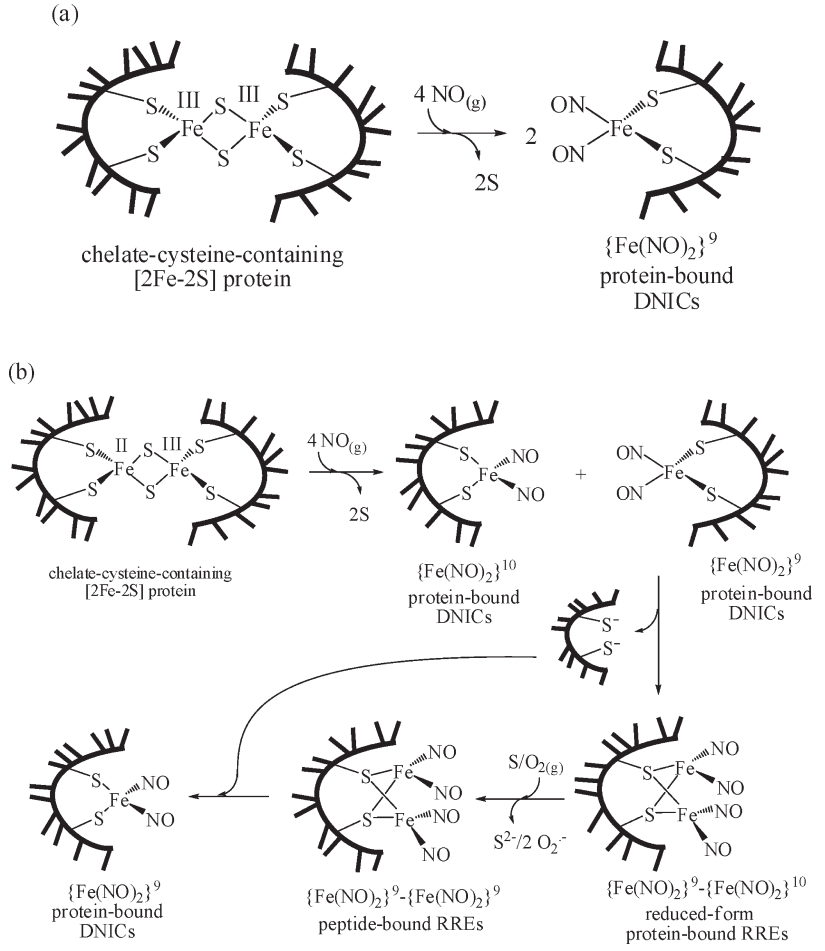

to the importance of cysteine residues being located in close proximity along the protein backbone in order to stabilize protein-bound DNICs over RREs. In particular, these results may signify that free-cysteine-bound DNICs are only derived from the transformation of protein-bound RREs in a biological system (Scheme 4). Also, this study signifies that nitrosylation of [Fe−S] proteins producing protein-bound RREs, reduced-form protein-bound RREs, or protein-bound DNICs in biological systems may be regulated by both the oxidation state of Fe and the chelating effect of the bound proteins of [Fe−S] clusters.

EXPERIMENTAL SECTION

Reagents and Chemicals. Manipulations, reactions, and transfers were conducted under N_2 according to Schlenk techniques or in a glovebox (N_2 gas). Solvents were distilled under N_2 from appropriate drying agents [diethyl ether from CaH_2; acetonitrile from CaH_2/P_2O_5; hexane and tetrahydrofuran (THF) from sodium benzophenone] and stored in dried, N_2-filled flasks over 4 Å molecular sieves. N_2 was purged through these solvents before use. Solvent was transferred to the reaction vessel via a stainless cannula under positive pressure of N_2. The reagents iron pentacarbonyl (Aldrich), sulfur powder (Showa), sodium nitrite (Fluka), 18-crown-6-ether (TCI), sodium hydroxide (Mallinckrodt), Fmoc-protected amino acids (Advanced Chemtech), Rink amide MBHA resin (0.5 mmol/g; Novabiochem), 1-hydroxybenzotriazole (Advanced Chemtech), 2-(1*H*-benzotriazol-1-yl)-1,1,3,3-tetramethyluronium hexafluorophosphate (Advanced Chemtech), piperidine (Alfa Aesar), *N*,*N*-dimethylformamide (Fisher), *N*-methyl-2-pyrolidinone (NMP; Mallinckrodt), triisopropylsilane (Alfa Aesar), 1,2-ethanedithiol (Acros), trifluoroacetic acid (TFA; Alfa Aesar), methyl *tert*-butyl ether (TEDIA), 5,5′-dithiobis(2-nitrobenzoic acid) (Alfa Aesar), and 4,4′-dipyridyl disulfide (Acros) were used as received. Complexes $[Na\text{-}18\text{-}crown\text{-}6\text{-}ether]_2[Fe_2(\mu\text{-}S)_2(NO)_4]$ and $Fe(CO)_2(NO)_2$ were synthesized and characterized as described in published literatures.[30] UV−vis spectra were recorded on a Jasco V-570 spectrometer. Analyses of carbon, hydrogen, and nitrogen were obtained with a CHN analyzer (Heraeus). ESI-MS spectra were obtained using a Varian 901 mass spectrometer.

Peptide Synthesis and Purification. All peptides were prepared on a 0.2 mmol scale by solid-phase Fmoc chemistry and standard reaction cycles on an automated PS3 peptide synthesizer (Protein Technologies Inc.). NMP was used as the major solvent in synthesis. The coupling time for each cycle was 4 h. Each peptide has an acetylated N-terminus. The use of a Rink amide resin with a MBHA linker generated an amidated C-terminus following cleavage from the resin with a 92.5% TFA/2.5% triisopropylsilane/2.5% H_2O/2.5% ethanedithiol solution. All peptides were purified by reverse-phase HPLC (Jasco) with a Thermo BioBasic semipreparative C_{18} column. H_2O/acetonitrile linear gradients with 0.1% (v/v) TFA as the counterion were used for the purification at a flow rate of 3 mL/min. The identities of all peptides were confirmed by using ESI-MS spectra: **C1A** observed 593, expected 593.34; **C2A** observed 664, expected 664.51; **C3A** observed

dx.doi.org/10.1021/ic201529e |*Inorg. Chem.* 2011, 50, 10417–10431

Scheme 9

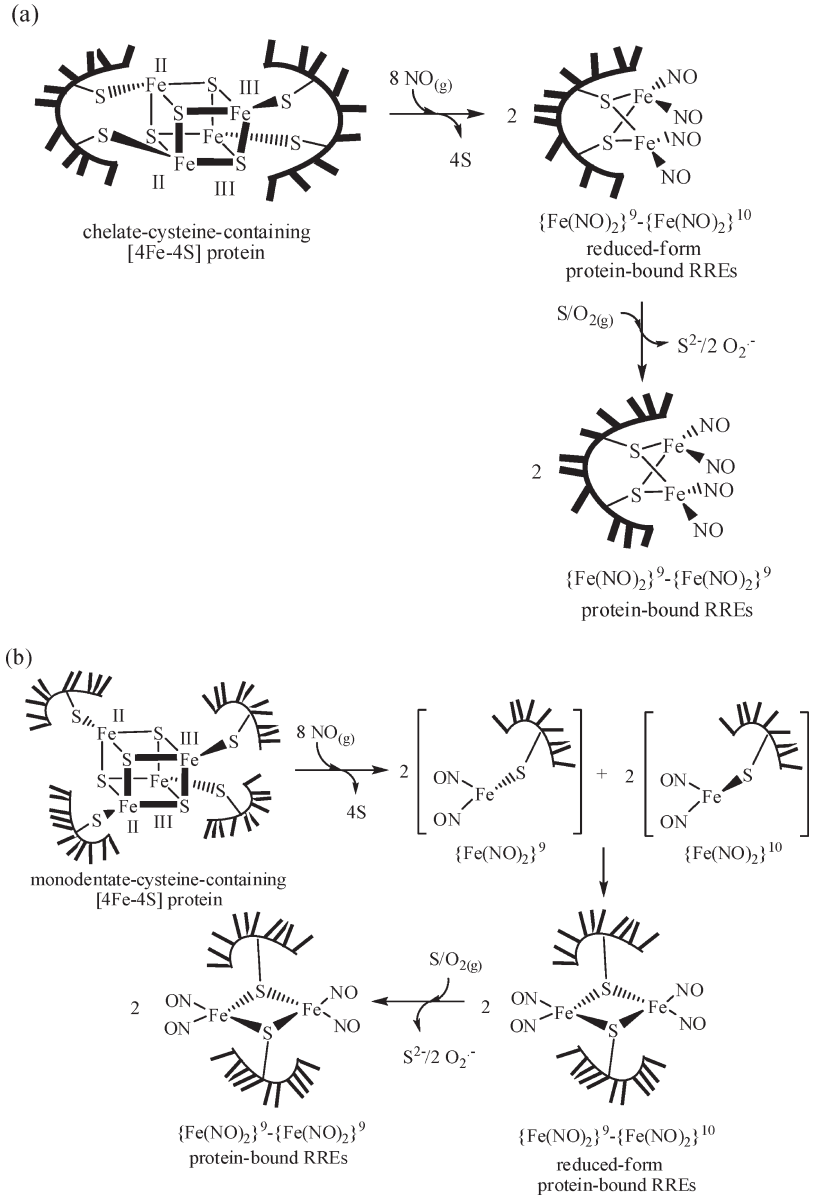

735, expected 735.20; **C4A** observed 806, expected 806.33. Peptide concentrations were determined by using a published assay with 4,4′-dipyridyl disulfide.[31]

Preparation of [Na-18-crown-6-ether][Fe(SPh-NO_2CO-OH)$_2$(NO)$_2$] (1). Complex [Na-18-crown-6-ether]$_2$[$Fe_2(\mu$-S)$_2$(NO)$_4$] (0.87 g, 1 mmol) and 5,5′-dithiobis(2-nitrobenzoic acid) (0.793 g, 2 mmol) were dissolved in CH_3CN (10 mL) and stirred for 30 min under nitrogen at ambient temperature. The reaction was monitored by FTIR. The IR ν_{NO} shifting from (1667 s, 1647 s cm^{-1}) to [1759 s, 1732 s, 1712 cm^{-1} (CH_3CN)] was assigned to the formation of complex **1**. Absorption spectrum (H_2O) [λ_{max}, nm (ε, M^{-1} cm^{-1})]: 400 (19 496). Anal. Calcd for $C_{26}H_{32}FeN_4NaO_{16}S_2$: C, 39.06; H, 4.03; N, 7.01. Found: C, 39.21; H, 4.33; N, 6.57. The reaction solution was dried under vacuum and then redissolved in THF/diethyl ether (1:1 volume ratio). The mixture solution was filtered through Celite to remove the insoluble solid, and hexane was then added to precipitate the dark-red solid **1** (1.28 g, 85%) characterized by IR and UV−vis spectra and single-crystal X-ray diffraction.

Preparation of Peptide-Bound DNICs C*n*A-DNIC (*n* = 1−4). To the 5 mL of phosphate buffer (20 mM, pH 8.5) of peptides [**C1A** (0.01 mmol), **C2A** (0.01 mmol), **C3A** (0.01 mmol), **C4A** (0.01 mmol), respectively] was added in a dropwise manner the 5 mL of phosphate buffer (20 mM, pH 8.5) of complex **1** (0.008 g, 0.01 mmol). The reaction solution was stirred under N_2 at ambient temperature for 1 h. The reaction was monitored by UV−vis spectra. The shift of the absorption maximum from 400 nm (complex **1**) to 412 nm implicated the complete reaction of complex **1** and peptide. The resulting yellow-brown solution was further purified by gel-filtration chromatography (Bio-Gel P-2 Gel, Bio Rad). The formation of peptide-bound DNICs was confirmed by the absorption spectra of the collected yellow fraction with the presence of two absorption bands [**C1A-DNIC** (309 sh, 413 nm), **C2A-DNIC** (313 sh, 409 nm), **C3A-DNIC** (315 sh, 407 nm), and **C4A-DNIC** (313 sh, 407 nm)] and by an EPR spectrum [g = 2.032 for **C1A-DNIC**; g = 2.029 for **C2A-DNIC**; g = 2.033 for **C3A-DNIC**; g = 2.029 for **C4A-DNIC** (H_2O)] at 298 K. The rhombic EPR g

values are $g_1 = 2.040$, $g_2 = 2.032$, $g_3 = 2.014$ for **C1A-DNIC**, $g_1 = 2.039$, $g_2 = 2.029$, $g_3 = 2.014$ for **C2A-DNIC**, $g_1 = 2.040$, $g_2 = 2.030$, $g_3 = 2.014$ for **C3A-DNIC**, $g_1 = 2.040$, $g_2 = 2.029$, $g_3 = 2.014$ for **C4A-DNIC** at 77 K. The peptide-bound DNICs were further characterized by ESI-MS: **C1A-DNIC** observed 708, expected 708.3; **C2A-DNIC** observed 779, expected 779.2; **C3A-DNIC** observed 850, expected 850.1; **C4A-DNIC** observed 921, expected 921.3, respectively. The solution was dried under vacuum, and the light-yellow solid was precipitated. The peptide-bound DNICs **C*n*A-DNIC** were also identified by aqueous solution IR {IR ν_{NO}: **C1A-DNIC** [1767 s, 1722 s cm^{-1} (H_2O)], **C2A-DNIC** [1768 s, 1722 s cm^{-1} (H_2O)], **C3A-DNIC** [1767 s, 1720 s cm^{-1} (H_2O)], **C4A-DNIC** [1766 s, 1721 s cm^{-1} (H_2O)].

Preparation of Monodenate-Cysteine-Containing Peptide-Bound RREs KCAAK-RRE and KCAAHK-RRE. The pure liquid $Fe(CO)_2(NO)_2$ (1.2 μL, 0.01 mmol) was added dropwise into the aqueous solution (5 mL) of peptide KCAAK (0.01 mmol) by a microsyringe, and then the mixture solution was stirred under N_2 at ambient temperature for 1 h. The reaction was monitored by aqueous solution IR and UV−vis spectra. The appearance of IR ν_{NO} stretching frequencies 1764 s, 1788 s, and 1820 w cm^{-1} (H_2O) and the electronic absorption bands of 312, 366, and 448 sh nm (H_2O) were consistent with the formation of peptide-bound RRE **KCAAK-RRE**. The red mixture solution was further purified by gel-filtration chromatography (Bio-Gel P-2 Gel, Bio Rad) and then dried under vacuum to precipitate the yellow solid **KCAAK-RRE**. The peptide-bound RRE **KCAAK-RRE** was also characterized by ESI-MS: **KCAAK-RRE** observed 1351, expected 1350. In a similar fashion, the reaction of peptide **KCAAHK** and $Fe(CO)_2(NO)_2$ (1:1 molar ratio) led to the formation of peptide-bound RRE **KCAAHK-RRE** characterized by IR [1764 s, 1788 s, 1820 w cm^{-1} (H_2O)], UV−vis [310, 364, 448 nm (H_2O)], and ESI-MS (observed 813, expected 1624).

Preparation of Chelate-Cysteine-Containing Peptide-Bound RREs C*n*A-RRE (*n* = 1−4). To the aqueous solution (5 mL) of peptide-bound DNICs **C*n*A-DNIC** [**C1A-DNIC** (0.0071 g, 0.01 mmol), **C2A-DNIC** (0.0078 g, 0.01 mmol), **C3A-DNIC** (0.0085 g, 0.01 mmol), **C4A-DNIC** (0.0092 g, 0.01 mmol), respectively] was added in a dropwise manner the pure liquid $Fe(CO)_2(NO)_2$ (1.2 μL, 0.01 mmol) at ambient temperature. The reaction solution was stirred at room temperature for $^1/_2$ h and monitored by UV−vis and EPR spectra. The shift of the electronic bands from (309 and 413 nm for **C1A-DNIC**, 313 and 409 nm for **C2A-DNIC**, 315 and 407 nm for **C3A-DNIC**, and 313 and 407 nm for **C4A-DNIC**) to (310, 369, 464, 613, and 952 nm for **rC1A-RRE**, 306, 368, 467, 646, and 957 nm for **rC2A-RRE**, 312, 367, 464, 639, and 939 nm for **rC3A-RRE**, 310, 370, 462, 637, and 950 nm for **rC4A-RRE**) in H_2O and the EPR g values [$g_\perp = 2.006$ and $g_\parallel = 1.970$ for **rC1A-RRE**, $g_1 = 2.012$, $g_2 = 1.999$, and $g_3 = 1.988$ for **rC2A-RRE**, $g_1 = 2.012$, $g_2 = 1.999$, and $g_3 = 1.989$ for **rC3A-RRE**, and $g_1 = 2.012$, $g_2 = 2.000$, and $g_3 = 1.988$ for **rC4A-RRE** at 77 K (H_2O)] implicated formation of the reduced peptide-bound RREs **rC*n*A-RRE** (*n* = 1−4). The reaction solution was then stirred for 1 min after O_2 gas was added to the mixture solution at ambient temperature. The electronic absorptions shifting to (312, 366, 448 sh nm) for **C1A-RRE**, (312, 364, 448 sh nm) for **C2A-RRE**, (314, 366, 448 sh nm) for **C3A-RRE**, (312, 364, 448 sh nm) for **C4A-RRE** and the disappearance of the EPR signal suggested formation of the peptide-bound RREs **C*n*A-RRE**. All peptide-bound RREs **C*n*A-RRE** were purified by gel-filtration chromatography (Bio-Gel P-2 Gel, Bio Rad) and also characterized by ESI-MS: **C1A-RRE** observed 823, expected 822; **C2A-RRE** observed 894, expected 893; **C3A-RRE** observed 965, expected 964; **C4A-RRE** observed 1036, expected 1035. IR ν_{NO} (H_2O): 1763 s, 1788 s, 1821 w cm^{-1} (**C1A-RRE**), 1764 s, 1788 s, 1822 w cm^{-1} (**C2A- RRE**), 1763 s, 1788 s, 1822 w cm^{-1} (**C3A- RRE**), and 1764 s, 1788 s, 1822 w cm^{-1} (**C4A-RRE**). The peptide-bound RREs **C*n*A-RRE** solution was dried under vacuum, and the yellow solid was precipitated.

Conversion of Peptide-Bound RREs C*n*A-RRE (*n* = 1−4)/KCAAK-RRE into Peptide-Bound DNICs C*n*A-DNIC (*n* = 1−4). Complex **KCAAK-RRE** (0.0135 g, 0.01 mmol) was treated with 2 equiv of peptide [**C1A** (0.118 g, 0.02 mmol), **C2A** (0.132 g, 0.02 mmol), **C3A** (0.146 g, 0.02 mmol), **C4A** (0.162 g, 0.02 mmol), respectively] in 5 mL of a phosphate buffer solution (20 mM, pH 8.5) at ambient temperature, and then the reaction solution was stirred at room temperature for 10 min. IR ν_{NO} shifting from 1764 s, 1788 s, 1820 w cm^{-1} (H_2O; **KCAAK-RRE**) to 1722 s, 1767 s, cm^{-1} (H_2O; **C1A-DNIC**) [(1722 s, 1768 s cm^{-1}) for **C2A-DNIC**, (1724 s, 1767 s cm^{-1}) for **C3A-DNIC**, (1723 s, 1766 s cm^{-1}) for **C4A-DNIC**], respectively, implicated the formation of the peptide-bound DNICs **C*n*A-DNIC**. The mixture solution was purified by gel-filtration chromatography (Bio-Gel P-2 Gel, Bio Rad) and further characterized by ESI-MS. In a similar fashion, the reaction of peptide-bound RREs **C1A-RRE** (or **C2A-RRE**) and peptide **C1A** (or **C2A**) in the ratio of 1:1 led to the formation of peptide-bound DNICs **C1A-DNIC** (or **C2A-DNIC**) characterized by IR and UV−vis.

Reaction of Peptide-Bound C1A-DNIC with Peptide C*n*A (*n* = 2−4). The peptide-bound DNIC **C1A-DNIC** (0.0071 g, 0.01 mmol) and peptide **C2A** (0.01 mmol) were mixed in 5 mL of phosphate buffer (20 mM, pH 8.5) and stirred under N_2 at room temperature for 10 min. The reaction was monitored by ESI-MS. The coexistence of peptide-bound DNICs **C1A-DNIC** and **C2A-DNIC** was characterized by ESI-MS. In a similar fashion, the reaction of **C1A-DNIC** and **C3A** also led to the formation of **C1A-DNIC** and **C3A-DNIC** identified by ESI-MS.

Conversion of Peptide-Bound RREs C*n*A-RRE (*n* = 1−4)/KCAAK-RRE into Cysteine-Bound DNIC $[Fe(Cys)_2(NO)_2]^-$. Peptide-bound RRE **KCAAK-RRE** (0.0135 g, 0.01 mmol) and L-cysteine (0.0051 g, 0.04 mmol) were dissolved in 5 mL pf phosphate buffer (20 mM, pH 8.5) and stirred under N_2 at ambient temperature for 5 min. The reaction was monitored by aqueous solution IR, UV−vis, and EPR spectra. The aqueous solution IR ν_{NO} shifting from [1764 s, 1788 s, 1823 w cm^{-1} (H_2O)] to [1727 s, 1772 s cm^{-1} (H_2O)] and the shift of electronic bands to (310, 405 nm) were assigned to formation of the cysteine-bound DNIC $[Fe(Cys)_2(NO)_2]^-$ with a well-resolved 13-line EPR spectrum (g value 2.031). In a similar fashion, the reaction of peptide-bound RREs **C*n*A-RRE** (*n* = 1−4) and L-cysteine (1:2 molar ratio) led to formation of the cysteine-bound DNIC $[Fe(Cys)_2(NO)_2]^-$ and peptide-bound DNICs **C*n*A-DNIC** (*n* = 1−4) characterized by IR, UV−vis, EPR, and ESI-MS.

Aqueous Solution IR Spectroscopy. The samples were dissolved in degassed water and sealed between two CaF_2 windows containing a 6 μm Teflon-separated spacer. IR spectra were collected using a Thermo Nicolet Nexus 470 spectrometer with a liquid-N_2-cooled Hg−Cd−Te detector. Spectra obtained from the accumulation of 100 scans and Fourier-transformed data were treated with Happ-Genzel apodization at a spectral resolution of 2 cm^{-1}.

EPR Spectroscopy. EPR spectra were performed at the X band using a Bruker EMX spectrometer equipped with a Bruker TE102 cavity. A flat cell was used to record EPR spectra at 298 K. The microwave frequency was measured with a Hewlett-Packard 5246 L electronic counter.

CD Spectroscopy. CD experiments were performed with an AVIV model 410 CD spectrometer. Far-UV CD spectra were obtained in phosphate buffer (20 mM, pH 7.4), using a 1-mm-path length quartz cuvette at 25 °C. The concentrations of peptide and peptide-bound DNICs were 100 μM in aqueous solution.

XAS Measurements and Data Analysis. All of the XAS experiments were done on the wiggler Beamline BL-17C at the NSRRC, Hsinchu, Taiwan. The incident X-ray photon energy was scanned using a double crystal Si(111) monochromator [beam size: 4 mm (H) × 2 mm (V)] with an incidence angle of 45° to the sample. The absorption spectra were collected in the fluorescence mode [$\mu(E) = I_F/I_0$] using a

Lytle detector with the sample maintained at a temperature of 283 K by a cold air jet stream. On the basis of comparisons of the first and last spectra recorded for a given sample, there is no photoreduction or radiation damage observed after repeated scans. The photon energy was calibrated with respect to the absorption edge (7112.0 eV) of a reference Fe foil, which was measured simultaneously with the sample.

The data analysis procedure was based on the previous report published by Li et al.[34c] The EXAFS $\chi(k)$ function (k = photoelectron wavenumber) was obtained after preedge and postedge background subtraction and normalization of the XAS data by the *AUTOBK* program.[32] $\chi(k)$ was then weighted by k^3 and Fourier-transformed into the R space as FT$[k^3\chi(k)]$ to separate the backscattering contributions from different neighboring atoms. For the fitting, S_0 was fixed at 0.85, which was determined by the best-fitting results of the known crystal structure of the DNIC sample. Then, the radial distribution profile was fitted in the range of $1.3 \leq R \leq 3.2$ Å with the variable parameters ΔE_0, R_j, σ_j^2, and N_j, using the *FEFFIT* program, where the backscattering amplitude and phase shift of specific atomic pairs were ab initio calculated by the FEFF7 code.[33,34] In the fitting, ΔE_0 was constrained to be the same for all scattering paths. Coordination numbers (N_j) were set to be a given value according to the standard crystallography structure of corresponding crystals. The quality of the data fitting was judged by the R_{fit} factor defined as

$$R_{\text{fit}} = \frac{\sum_{j=1}^{n}\{[\text{Re}(f_j)]^2 + [\text{Im}(f_j)]^2\}}{\sum_{j=1}^{n}\{[\text{Re}(\tilde{\chi}_{\text{data}\,j})]^2 + [\text{Im}(\tilde{\chi}_{\text{data}\,j})]^2\}} \quad (1)$$

where $\tilde{\chi} = k^3\chi$ and n is the number of evaluations of f_j, with $f_j = \tilde{\chi}_{\text{data}\,j} - \tilde{\chi}_{\text{model}\,j}$ (and, hence, R_{fit}), minimized in the nonlinear least-squares fitting algorithm.

Crystallography. Crystallographic data and structural refinement parameters of complex **1** are summarized in Table S1 in the SI. The crystal chosen for X-ray diffraction studies measured $0.18 \times 0.07 \times 0.02$ mm^3 for complex **1**. The crystal was mounted on a glass fiber and quickly coated in epoxy resin. Unit cell parameters were obtained by least-squares refinement. Diffraction measurements for complex **1** were carried out on a Bruker X8 APEX II CCD diffractometer with graphite-monochromatized Mo Kα radiation (λ = 0.7107 Å) between 1.77° and 26.39° for complex **1**. The positional and anisotropic thermal parameters of all non-H and H atoms of least-squares refinement were fixed at calculated positions and refined at riding modes. A multiscan absorption correction was made. The *SHELXTL* structure refinement program was employed.[35]

■ ASSOCIATED CONTENT

Supporting Information. X-ray crystallographic files in CIF format and the structure determination of [Na-18-crown-6-ether][Fe(SPhNO$_2$COOH)$_2$(NO)$_2$], parameters used in fitting the k^3-weighted EXAFS data, and ESI-MS, IR, UV−vis, EPR, CD, and EXAFS spectra. This material is available free of charge via the Internet at http://pubs.acs.org.

■ AUTHOR INFORMATION

Corresponding Author
*E-mail: wfliaw@mx.nthu.edu.tw.

■ ACKNOWLEDGMENT

We gratefully acknowledge financial support from the National Science Council of Taiwan. The authors thank Pei-Lin Chen for single-crystal X-ray structural determinations and Juo-Chi Chen (National Tsing Hua University, Hsinchu, Taiwan) for EPR measurements.

■ REFERENCES

(1) (a) Toledo, J. C., Jr.; Bosworth, C. A.; Hennon, S. W.; Mahtani, H. A.; Bergonia, H. A.; Lancaster, J. R., Jr. *J. Biol. Chem.* **2008**, *283*, 28926–28933. (b) Landry, A. P.; Duan., X. D.; Huang, H.; Ding, H. *Free Radical Biol. Med.* **2011**, *50*, 1582–1590. (c) Duan, X.; Yang, J.; Ren, B.; Tan, G.; Ding, H. *Biochem. J.* **2009**, *417*, 783–789.

(2) (a) Ueno, T.; Susuki, Y.; Fujii, S.; Vanin, A. F.; Yoshimura, T. *Biochem. Pharmacol.* **2002**, *63*, 485–493. (b) Foster, M. W.; Hess, D. T.; Stamler, J. S. *Trends Mol. Med.* **2009**, *15*, 391–404. (c) Hess, D. T.; Matusmoto, A.; Kim, S.-O.; Marshall, H. E.; Stamler, J. S. *Nat. Rev. Mol. Cell Biol.* **2005**, *6*, 150–166. (d) Foster, M. W.; McMahon, T. J.; Stamler, J. S. *Trends Mol. Med.* **2003**, *9*, 160–168.

(3) (a) Palmer, R. M. J.; Ferrige, A. G.; Moncada, S. *Nature* **1987**, *327*, 524–526. (b) Ignarro, L. J.; Buga, G. M.; Wood, K. S.; Byrns, R. E.; Chaudhuri, G. *Proc. Natl. Acad. Sci. U.S.A.* **1987**, *84*, 9265–9269. (c) Alderton, W. K.; Cooper, C. E.; Knowles, R. G. *Biochem. J.* **2001**, *357*, 593–615. (d) Butler, A. R.; Megson, I. L. *Chem. Rev.* **2002**, *102*, 1155–1166. (e) Szaciłowski, K.; Chmura, A.; Stasicka, Z. *Coord. Chem. Rev.* **2005**, *249*, 2408–2436. (f) Lorsbach, R. B.; Murphy, W. J.; Lowenstein, C. J.; Snyder, S. H.; Russell, S. W. *J. Biol. Chem.* **1993**, *268*, 1908–1913.

(4) (a) Foster, M. W.; Cowan, J. A. *J. Am. Chem. Soc.* **1999**, *121*, 4093–4100. (b) Cooper, C. E. *Biochim. Biophys. Acta* **1999**, *1411*, 290–309.

(5) (a) Nagane, R.; Koshigoe, T.; Chikira, M.; Long, E. C. *J. Inorg. Biochem.* **2001**, *83*, 17–23. (b) Mulholland, S. E.; Gibney, B. R.; Rabanal, F.; Dutton, P. L. *J. Am. Chem. Soc.* **1998**, *120*, 10296–10302. (c) Korendovych, I. V.; Senes, A.; Kim, Y. H.; Lear, J. D.; Fry, H. C.; Therien, M. J.; Blasie, J. K.; Walker, F. A.; DeGrado, W. F. *J. Am. Chem. Soc.* **2010**, *132*, 15516–15518. (d) Rathinakumar, R.; Wimley, W. C. *J. Am. Chem. Soc.* **2008**, *130*, 9849–9858. (e) Ghosh, D.; Pecoraro, V. L. *Inorg. Chem.* **2004**, *43*, 7902–7915. (f) Reddi, A. R.; Guzman, T. R.; Breece, R. M.; Tierney, D. L.; Gibney, B. R. *J. Am. Chem. Soc.* **2007**, *129*, 12815–12827. (g) Cline, D. J.; Thorpe, C.; Schneider, J. P. *J. Am. Chem. Soc.* **2003**, *125*, 2923–2929.

(6) (a) Jones, A. K.; Lichtenstein, B. R.; Dutta, A.; Gordon, G.; Dutton, P. L. *J. Am. Chem. Soc.* **2007**, *129*, 14844–14845. (b) Petros, A. K.; Reddi, A. R.; Kennedy, M. L.; Hyslop, A. G.; Gibney, B. R. *Inorg. Chem.* **2006**, *45*, 9941–9958. (c) Oda, T.; Nagao, H.; Sugiyama, A.; Wada, K. *Polyhedron* **2005**, *24*, 2550–2556. (d) Doerr, A.; McLendon, G. L. *Inorg. Chem.* **2004**, *43*, 7916–7925.

(7) (a) Iranzo, O.; Ghosh, D.; Pecoraro, V. L. *Inorg. Chem.* **2006**, *45*, 9959–9973. (b) Matzapetakis, M.; Farrer, B. T.; Weng, T.-C.; Hemmingsen, L.; Penner-Hahn, J. E.; Pecoraro, V. L. *J. Am. Chem. Soc.* **2002**, *124*, 8042–8054. (c) Petros, A. K.; Shaner, S. E.; Costello, A. L.; Tierney, D. L.; Gibney, B. R. *Inorg. Chem.* **2004**, *43*, 4793–4795. (d) Chung, K. C. C.; Cao, L.; Dias, A. V.; Pickering, I. J.; George, G. N.; Zamble, D. B. *J. Am. Chem. Soc.* **2008**, *130*, 14056–14057. (e) Lee, K.-H.; Matzapetakis, M.; Mitra, S.; Marsh, E. N. G.; Pecoraro, V. L. *J. Am. Chem. Soc.* **2004**, *126*, 9178–9179.

(8) (a) Laplaza, C. E.; Holm, R. H. *J. Am. Chem. Soc.* **2001**, *123*, 10255–10264. (b) Kharenko, O. A.; Ogawa, M. Y. *J. Inorg. Biochem.* **2004**, *98*, 1971–1974. (c) Kennedy, M. L.; Petros, A. K.; Gibney, B. R. *J. Inorg. Biochem.* **2004**, *98*, 727–732. (d) Kharenko, O. A.; Kennedy, D. C.; Demeler, B.; Maroney, M. J.; Ogawa, M. Y. *J. Am. Chem. Soc.* **2005**, *127*, 7678–7679.

(9) Kennedy, M. L.; Gibney, B. R. *J. Am. Chem. Soc.* **2002**, *124*, 6826–6827.

(10) (a) Chakraborty, S.; Touw, D. S.; Peacock, A. F. A.; Stuckey, J.; Pecoraro, V. L. *J. Am. Chem. Soc.* **2010**, *132*, 13240–13250. (b) Farrer, B. T.; McClure, C. P.; Penner-Hahn, J. E.; Pecoraro, V. L. *Inorg. Chem.* **2000**, *39*, 5422–5423.

(11) Fry, H. C.; Lehmann, A.; Saven, J. G.; DeGrado, W. F.; Therien, M. J. *J. Am. Chem. Soc.* **2010**, *132*, 3997–4005.

(12) (a) Welter, R.; Yu, L.; Yu, C.-A. *Arch. Biochem. Biophys.* **1996**, *331*, 9–14. (b) Rogers, P. A.; Eide, L.; Klungland, A.; Ding, H. *DNA*

Repair **2003**, *2*, 809–817. (c) Sellers, V. M.; Johnson, M. K.; Dailey, H. A. *Biochemistry* **1996**, *35*, 2699–2704.

(13) Yukl, E. T.; Elbaz, M. A.; Nakano, M. M.; Pierre, M.-L. *Biochemistry* **2008**, *47*, 13084–13092.

(14) (a) Ding, H.; Demple, B. *Proc. Natl. Acad. Sci. U.S.A.* **2000**, *97*, 5146–5150. (b) Yang, W.; Rogers, P. A.; Ding, H. *J. Biol. Chem.* **2002**, *277*, 12868–12873.

(15) (a) Tinberg, C. E.; Tonzetich, Z. J.; Wang, H.; Do, L. H.; Yoda, Y.; Cramer, S. P.; Lippard, S. J. *J. Am. Chem. Soc.* **2010**, *132*, 18168–18176. (b) Harrop, T. C.; Tonzetich, Z. J.; Reisner, E.; Lippard, S. J. *J. Am. Chem. Soc.* **2008**, *130*, 15602–15610. (c) Tonzetich, Z. J.; Do, L. H.; Lippard, S. J. *J. Am. Chem. Soc.* **2009**, *131*, 7964–7965.

(16) Crack, J. C.; Smith, L. J.; Stapleton, M. R.; Peck, J.; Watmough, N. J.; Buttner, M. J.; Buxton, R. S.; Green, J. G.; Oganesyan, V. O.; Thomson, A. J.; Le Brun, N. E. *J. Am. Chem. Soc.* **2011**, *133*, 1112–1121.

(17) (a) Tsai, M.-C.; Tsai, F.-T.; Lu, T.-T.; Tsai, M.-L.; Wei, Y.-C.; Hsu, I.-J.; Lee, J.-F.; Liaw, W.-F. *Inorg. Chem.* **2009**, *48*, 9579–9591. (b) Huang, H.-W.; Tsou, C.-C.; Kuo, T.-S.; Liaw, W.-F. *Inorg. Chem.* **2008**, *47*, 2196–2204. (c) Tsai, M.-L.; Liaw, W.-F. *Inorg. Chem.* **2006**, *45*, 6583–6585. (d) Tsai, F.-T.; Chiou, S.-J.; Tsai, M.-C.; Tsai, M.-L.; Huang, H.-W.; Chiang, M.-H.; Liaw, W.-F. *Inorg. Chem.* **2005**, *44*, 5872–5881. (e) Costanzo, S.; Ménage, S.; Purrello, R.; Bonomo, R. P.; Fontecave, M. *Inorg. Chim. Acta* **2001**, *318*, 1–7.

(18) (a) Lu, T.-T.; Tsou, C.-C.; Huang, H.-W.; Hsu, I.-J.; Chen, J.-M.; Kuo, T.-S.; Wang, Y.; Liaw, W.-F. *Inorg. Chem.* **2008**, *47*, 6040–6050. (b) Tsou, C.-C.; Lu, T.-T.; Liaw, W.-F. *J. Am. Chem. Soc.* **2007**, *129*, 12626–12627.

(19) (a) Tsai, F.-T.; Kuo, T.-S.; Liaw, W.-F. *J. Am. Chem. Soc.* **2009**, *131*, 3426–3427. (b) Tsai, F.-T.; Chen, P.-L.; Liaw, W.-F. *J. Am. Chem. Soc.* **2010**, *132*, 5290–5299.

(20) Zhang, L.; Goldammer, C.; Henkel, B.; Zuhl, F.; Panhaus, G.; Jung, G.; Bayer, E. In *InnoVation and PerspectiVe in Solid-Phase Synthesis*; Epton, R., Ed.; Mayflower: Birmingham, U.K., 1994; pp 711−716.

(21) Lu, T.-T.; Chiou, S.-J.; Chen, C.-Y.; Liaw, W.-F. *Inorg. Chem.* **2006**, *45*, 8799–8806.

(22) Lu, T.-T.; Lai, S.-H.; Li, Y.-W.; Hsu, I.-J.; Jang, L. Y.; Lee, J.-F.; Chen, I.-C.; Liaw, W.-F. *Inorg. Chem.* **2011**, *50*, 5396–5406.

(23) Lu, T.-T.; Huang, H.-W.; Liaw, W.-F. *Inorg. Chem.* **2009**, *48*, 9027–9035.

(24) D'Autréaux, B.; Horner, O.; Oddou, J.-L.; Jeandey, C.; Gambarelli, S.; Berthomieu, C.; Latour, J.-M.; Michaud-Soret, I. *J. Am. Chem. Soc.* **2004**, *126*, 6005–6016.

(25) Tonzetich, Z. J.; Wang, H.; Mitra, D. M.; Tinberg, C. E.; Do, L. H.; Jenney, F. E. J., Jr.; Adams, M. W. W.; Cramer, S. P.; Lippard, S. J. *J. Am. Chem. Soc.* **2010**, *132*, 6914–691.

(26) McDonald, C. C.; Phillips, W. D.; Mower, H. F. *J. Am. Chem. Soc.* **1965**, *87*, 3319–3326.

(27) (a) Figgis, B. N.; Hitchman, M. A. *Ligand Field Theory and Its Applications*; Wiley-VCH: New York, 2000; pp 181−183. (b) Westre, T. E.; Kennepohl, P.; DeWitt, J. G.; Hedman, B.; Hodgson, K. O.; Solomon, E. I. *J. Am. Chem. Soc.* **1997**, *119*, 6297–6314.

(28) Tsai, M.-L.; Chen, C.-C.; Hsu, I. J.; Ke, S.-C.; Hsieh, C.-H.; Chiang, K.-A.; Lee, G.-H.; Wang, Y.; Chen, J.-M.; Lee, J.-F.; Liaw, W.-F. *Inorg. Chem.* **2004**, *43*, 5159–5167.

(29) Thomas, J. T.; Robertson, J. H.; Cox, E. G. *Acta Crystallogr.* **1958**, *11*, 599–604.

(30) (a) Sanina, N. A.; Filipenko, O. S.; Aldoshin, S. M.; Ovanesyana, N. S. *Russ. Chem. Bull.* **2000**, *49*, 1109–1112. (b) Heiber, W.; Beutner, H.; Anorg., Z. *Allgen. Chem.* **1963**, *320*, 101.

(31) Mantle, M.; Stewart, G.; Zayas, G.; King, M. *Biochem. J.* **1990**, *266*, 597–604.

(32) Frenkel, A.; Stern, E. A.; Voronel, A.; Qian, M.; Newville, M. *Phys. Rev. B* **1994**, *49*, 11662.

(33) (a) Hsu, I.-J.; Liu, R.-S.; Chen, J.-M.; Liu, R.-G.; Jang, L.-Y.; Lee, J.-F.; Harris, K. D. M. *Chem. Mater.* **2000**, *12*, 1115–1121. (b) Hsu, I.-J.; Shiu, Y.-J.; Jeng, U. S.; Chen, T.-H.; Huang, Y.-S.; Lai, L.-N.; Jang, L.-Y.; Lee, J.-F.; Lin, L.-J.; Lin, S.-H.; Wang, Y. *J. Phys. Chem. A* **2007**, *111*, 9286–9290. (c) Li, M.; Huang, Y.-S.; Jeng, U.-S.; Hsu, I.-J.; Wu, Y.-S.; Lai, Y.-H.; Su, C.-H.; Lee, J.-F.; Wang, Y.; Chang, C.-C. *Biophys. J.* **2009**, *97*, 609–617.

(34) Newville, M.; Ravel, B.; Haskel, D.; Rehr, J. J.; Stern, E. A. *Physica B* **1995**, *208*, 154–159.

(35) Sheldrick, G. M. *SHELXTL, Program for Crystal Structure Determination*; Siemens Analytical X-ray Instruments Inc.: Madison, WI, 1994.